

Contents lists available at ScienceDirect

Acta Biomaterialia

journal homepage: www.elsevier.com/locate/actbio



Full length article

Effective easing of the side effects of copper intrauterine devices using ultra-fine-grained Cu-0.4Mg alloy



Qianqian Fan^{a,1}, Guo Bao^{b,1}, Dongfeng Ge^a, Kun Wang^a, Mingming Sun^a, Tingting Liu^a, Jianing Liu^c, Zechuan Zhang^c, Xiangbo Xu^a, Xiaoxue Xu^{d,*}, Bin He^{b,*}, Jiancun Rao^{e,*}, Yufeng Zheng^{a,c,*}

- ^a Graduate School of Peking Union Medical College, Beijing 100730, China
- ^b Department of Reproduction and Physiology, National Research Institute for Family Planning, Beijing 100081, China
- ^c Department of Materials Science and Engineering, College of Engineering, Peking University, Beijing 100871, China
- ^d Institute for Biomedical Materials and Devices, Faculty of Science, University of Technology Sydney, NSW 2007, Australia
- ^e AIM Lab, Maryland NanoCenter, University of Maryland, College Park, MD 20742, USA

ARTICLE INFO

Article history: Received 14 December 2020 Revised 11 April 2021 Accepted 16 April 2021 Available online 24 April 2021

Keywords:
Ultrafine grained bulk copper
Copper-magnesium alloy
Biocorrosion
Burst release rate
Intrauterine implantation
Biocompatibility

ABSTRACT

Copper intrauterine device is one of the most adopted contraceptive methods with high effectiveness (over 99 %), low cost, spontaneous reversibility and long-lasting usage. However, the side effects induced from the initial burst release of copper ions (Cu²⁺) hinder the continuation of the Cu-IUD made of Coarse-Grained Copper (CG Cu). We proposed to tailor the bio-corrosion behaviors of better control of Cu²⁺ release via the addition of bioactive Mg into the Ultra-Fine Grained (UFG) Bulk Cu. Thus, UFG bulk Cu with 0.4 wt.% Mg was produced via equal-channel angular pressing. The microstructures of the UFG Cu-0.4Mg was observed using electron backscatter diffraction and transmission electron microscopy techniques. The in vitro long-term corrosion behaviors in simulated uterine fluid, cytotoxicity to four cell lines, in vivo biocompatibility and contraceptive efficacy were all studied on CG Cu, UFG Cu and UFG Cu-0.4Mg materials. The results demonstrate that both the ultrafine grains and the addition of bioactive Mg into Cu contribute to the suppression of the burst release of Cu²⁺ in the initial stage and the maintenance of high level Cu²⁺ in long-term release. Moreover, the UFG Cu-0.4Mg also exhibited much improved cell and tissue biocompatibility from both the in vitro and in vivo evaluations. Therefore, the contraceptive efficacy of UFG Cu-0.4Mg is still maintained as high as the CG Cu and UFG Cu while the side effects are significantly eased, suggesting the high potential of the UFG Cu-0.4Mg alloy as a new upgrading or alternative material for Cu-IUD.

Statement of significance

The side effects from burst release of Cu²⁺ at the initial implantation stage of Cu-containing intrauterine devices (Cu-IUD) is one of the main drawbacks of these devices. In this work, an ultra-fine-grained Cu (UFG Cu) alloyed with a low amount of bioactive Mg was used for a Cu-IUD. The UFG Cu-0.4Mg alloy exhibited suppressed burst release of Cu²⁺ at initial implantation, while active Cu²⁺ release for long-term usage was maintained, comparable to coarse-grained pure Cu. Furthermore, the UFG Cu-0.4Mg alloy displayed significantly improved biocompatibility with human uterus cells and a much decreased inflammatory response within the uterus. Therefore, the side effects from Cu-IUD were eased, while high antifertility efficacy of the UFG Cu-0.4Mg alloy was maintained. The UFG Cu-0.4Mg alloy is promising for Cu-IUD.

 $\ensuremath{\mathbb{C}}$ 2021 Acta Materialia Inc. Published by Elsevier Ltd. All rights reserved.

* Corresponding authors.

E-mail addresses: Xiaoxuehelen.xu@uts.edu.au (X. Xu), hebin@nrifp.org.cn (B. He), jcrao@umd.edu (J. Rao), yfzheng@pku.edu.cn (Y. Zheng).

¹ Contribute equally as first author.

1. Introduction

The non-hormonal copper-containing Intrauterine Devices (Cu-IUD) is one of the most widely used contraceptive methods [1] with advantages of great safety, high effectiveness, low cost and

reversible long-lasting contraception [2-4]. The action mechanism of Cu-IUDs could be attributed to the antifertility agent cupric ions (Cu²⁺) that is daily released from the bulk copper in uterine secretions. Cu²⁺ exerts the contraceptive action by (1) decreasing the sperm motility and viability and (2) enhancing the inflammatory response in the uterine cavity to prevent the formation of viable embryos. Moreover, it is believed that excess Cu²⁺ can cause both genotoxicity and cytotoxicity, and further alter the expression level of genes related to endometrial receptivity and immune response [5–7]. Thus, the release rate of Cu^{2+} from Cu corrosion process is critically important not only for Cu-IUD efficacy, but also for the overall performance. For example, over released Cu²⁺, up to 296 µg/day, i.e., burst release, from a newly implanted Cu-IUD [1], could induce irregular vaginal bleeding, cramping, pelvic inflammatory disease, expulsion and lumbosacral pain during the first implanted month [8-10]. It is reported that the excessive Cu²⁺ above 20 µM could drastically increase the contraction of uterine smooth muscle, eliciting the spontaneous contractile activity. While the concentration higher than 80 µM, Cu²⁺ would produce muscle spasmodic contracture [11], which could be a reason for the cramping pain when Cu²⁺ is burst released. On the other hand, the sufficient and sustainable release of Cu²⁺ after 5-10 years corrosion is essentially required for contraception activity of Cu-IUD. In the later stage of Cu-IUD usage, the Cu surface would be fully covered with thick corrosion products and deposition like calcites from the uterus luminal fluids, so the Cu²⁺ releasing rate could be lower than 2 µg/day which is reported as the minimum amount for effective contraception [1]. Ideally, a constant and appropriate release rate of Cu^{2+} in uterine should be maintained over the life span for Cu-IUD. Hence, the corrosion behavior of the Cu for IUD must be tuned with the minimized burst release but elevated longterm release of Cu²⁺.

Extrinsic modifications were carried out to the IUD Cu materials to overcome the issues related to Cu²⁺ release. For instance, smaller Cu balls were threaded over a shape memory alloy wire [12] to replace T-shaped Cu tubes for reduced Cu²⁺ burst release amount. Pretreatment on Cu surfaces with organic corrosion inhibitors also showed modified corrosion performances of Cu-IUD [13,14]. Cu alloys with Al (70Cu-26Zn-4Al) was proposed as a substitute for the bulk pure Cu as the alloy surface could form a compact protective Al₂O₃ layer to reduce the burst release [15]. However, the introduced extrinsic factors, such as the alloy elements, or surface coatings, induced extra effects, such as toxicity of Ni element [12] and the uncertainty of long-term Cu²⁺ release with Al₂O₃ layer [15]. A new type of Cu nanocomposite, Cu micro/nanoparticles within the dense and porous Low-Density Polyethylene (Cu/LDPE), have been developed for Cu-IUD [16–18]. The Cu²⁺ release rate depended on the Cu particles concentration and their dissolution. The burst release still presented and the long-term release was quite low, limiting the lifetime of IUD. Similarly, Zn and ZnO nanoparticles incorporated into the LDPE composite were also considered for IUD contraception [19,20].

Zheng's group adopted UFG Cu firstly for Cu-IUD and achieved much reduced burst release and well-maintained long-term release of Cu²⁺ [21,22]. The UFG Cu with high density of grain boundaries induced the uniform distribution of surface free energy and facilitated the formation of the uniform and dense protective layers on the corroded surface. The ultrafine grained bulk metallic materials via Severe Plastic Deformation (SPD) have been applied in biomedical areas comprehensively both with enhanced mechanical properties and with improved bio-corrosion and biocompatibility, including UFG Ti and its alloys [23,24], UFG stainless steel [25], UFG Zr [26] and UFG degradable Mg [27].

In order to further reduce the burst release of Cu²⁺ and ease the side effects of IUD, the present work proposed to alloy a bioactive metal of Mg into the UFG Cu. Mg²⁺ is not only an essential element in human body [28] participating in the metabolism of many biomolecules, including glucids, lipids, proteins, and nucleic acids, but also one of the most important cations in cells and plays multiple roles in enzyme processes, such as modulation of calcium and potassium ion channels, cell proliferation and apoptosis [29]. Mg²⁺ is also thought to be an anti-inflammatory agent because levels of magnesium in the body are inversely correlated to levels of inflammatory markers [30]. Furthermore, Mg salts are used as uterine relaxants in clinic and magnesium sulfate has been clinically used for the management of severe preeclampsia [31,32]. Previous works on the bioactive Mg metal and its alloys for bone implants and cardiovascular intervention materials demonstrated Mg as a highly potential biomedical material with controllable biodegradability, excellent mechanical strength, and mild inflammatory response [28,34]. Thus, alloying Mg into Cu could be very biocompatible at the same time to further improve the burst release of Cu²⁺ by the preferential dissolution of Mg compared to Cu. In the present work, together with the UFG Cu and the CG Cu, we studied the UFG Cu-0.4Mg in the physical, chemical and biomedical properties for the purpose of IUD employment. The relationship was comprehensively discussed between the microstructure and composition with the properties including the corrosion behaviors, in vitro cytocompatibility, in vivo tissue-compatibility, and contraceptive efficacy.

2. Materials and methods

2.1. Materials

The commercial pure CG Cu rods (d = 10 mm, 99.99 %) was purchased from Yunnan Kuntong Co. Ltd., China. UFG Cu rods (d = 16 mm) produced via 8-pass Equal Channel Angular Pressing (ECAP) was obtained from Wujiang Yongyuan technology Co. Ltd., China [21]. The UFG Cu-0.4Mg rods (d=12 mm) was produced via 8-pass Equal Channel Angular Pressing (ECAP) from Harbin Engineering University, China. The three Cu materials were cut into circular shaped disks with a diameter of 9 mm and a thickness of 1 mm and the elemental composition of the three materials were shown in Table S1.

2.2. Microstructure characterization

In order to confirm the grain size of the CG Cu, UFG Cu and UFG Cu-Mg, Electron Backscatter Diffraction (EBSD) was employed to characterize the grain size, grain orientation, and grain boundary distributions. Prior to all measurements, the three samples were mechanically ground with 1200 grit silicon carbide abrasive paper followed by polishing with 3 μm and 50 nm $\rm SiO_2$ suspension in sequence. The polished samples were then subjected to a Gatan PECS II broad ion miller for final surface polishing. The EBSD analysis was performed in a rectangular area with scanning step of 50 nm in a ThermoFisher (FEI) Helios G4 PFIB UXe DualBeam Scanning Electron Microscope (SEM) equipped with an EBSD analyzer "CHANNEL 5". The acquired results were analyzed using the AZtec software.

The microstructures of the Cu materials were also performed using Transmission Electron Microscopy (TEM). Thin discs cut from these Cu-containing materials were mechanically ground and polished. Subsequently, from these finely polished discs, TEM specimens were prepared by *in-situ* lift-out technique in a dual-beam system (Tescan GAIA3) and further thinned to about 100 nm thick by Focused Ion Beam (FIB) of Ga⁺ at 5 kV, 15 pA. The TEM study was carried out in a JEM 2100F equipped with Bruker EDS and Gatan EELS/GIF systems operating at 200 keV.

2.3. Electrochemical tests

The electrochemical corrosion properties of the CG Cu, UFG Cu and UFG Cu-0.4Mg were carried out in simulated uterine fluid (SUF) (NaCl 4.97 g/L, KCl 0.224 g/L, CaCl₂ 0.167 g/L, NaHCO₃ 0.25 g/L, Glucose 0.50 g/L, NaH₂PO4·2H₂O 0.072 g/L) [35] solution at 37 ± 0.5°C using an electrochemical workstation (Metrohm Ltd., Switzerland). All specimens were polished with SiC paper to 2000 grit and then ultrasonically cleaned in acetone and ethanol for 15 min, respectively. A three-electrode system was used with a saturated calomel electrode as the reference electrode, a platinum electrode as the auxiliary electrode, and the Cu specimen served as the working electrode. The exposure area of the specimen was 0.242 cm². Open Circuit Potential (OCP) for Cu specimen was performed firstly for approximately 1 h. Then potentiodynamic polarization tests were conducted at a scanning rate of 0.5 mV/s and the potential scan range of -0.5 to 0.5 V vs SCE at 37°C. Corrosion parameters including corrosion potential (Ecorr) and corrosion current density (i_{corr}) were calculated from the polarization curves by Tafel analysis based on the polarization plots. Five disks for each kind of Cu material were tested and the obtained data was analyzed using Nova 1.11.

2.4. Long term immersion test

In order to investigate the *in vitro* long-term corrosion behaviors of Cu materials, the immersion tests of the polished CG Cu, UFG Cu and UFG Cu-0.4Mg specimens in SUF at 37°C were conducted for 300 days. The ratio of SUF volume to the Cu exposure surface area was 20 mL/cm^2 for each sample. The initial pH value of the SUF was set at 7.0. The pH values (PB-10, Sartorius) of the SUF and the released Cu²⁺ and Mg²⁺ during the immersion tests were monitored by sampling 5 mL of the SUFs at the time points of 1, 10, 15, 20, 25, 30, 45, 60, 90, 120, 150, 180, 210, 240, 270 and 300 days, respectively. Both the Cu²⁺ and Mg²⁺ concentrations were analyzed using ICP-MS (iCAP6300, Thermo Scientific) and the release rate of accumulated metallic ion was calculated out with the unit of μ g/day. The release rate data was then converted to a copper surface area of 200 mm² for direct comparison with the data from typical Cu-IUD200 with 200 mm² surface area [35].

The corrosion rate of each kind of Cu material was calculated out. After being immersed for 1, 10, 30, 60, 150 and 300 days, four samples from each Cu material were taken out of the SUF solution, rinsed with distilled water and dried in air. The corrosion products were removed according to the standard protocol [36] by immersing the Cu materials in the concentrated hydrochloric acid for 5 min. The weight loss of each Cu material is the difference between the mass before and after the immersion in the SUF. So the corrosion rate can be obtained using the following equation [37]:

$$C = \frac{\Delta m}{\rho \times A \times t} \tag{1}$$

where C is the corrosion rate in mm/year, Δm is the weight loss, ρ is the density of the Cu material, A is the initial implant surface area, and t is the implantation time.

2.5. Corrosion morphology and product characterizations

The corrosion morphology of the long-term immersed Cu materials was observed in SEM (S-4800, Hitachi) and its elemental composition was studied with the equipped Energy-Disperse X-ray Spectroscopy (EDS). The phase constitution of the corrosion products was also analyzed using the X-ray diffraction technique (Rigaku D/MAX 2400) with Cu K α radiation powered at 40 kV and the scan rate of 4 °/min from 20~80 °.

2.6. In vitro biomedical studies

2.6.1. Cell culture and cell immunofluorescence

Four cell lines were adopted for the CG Cu, UFG Cu and UFG Cu-0.4Mg materials on in vitro biomedical studies. Human Umbilical Vein Endothelial Cells (HUVEC) and Murine fibroblast cells (L-929) were cultured in Dulbecco's Modified Eagle's Medium (DMEM) containing 10 % fetal bovine serum, 100 U/mL penicillin and 100 ug/mL streptomycin. Primary Human Endometrial Epithelial Cells (HEEC) and primary Human Endometrial Stromal Cells (HESC) were purchased from Shenzhen Procell Company, China and cultured in DMEM (Nutrient Mixture F-12 (DMEM/F12) with 10 % fetal bovine serum, 100 U/mL penicillin and 100 ug/mL streptomycin). All experimental cell lines were cultured in a humidified atmosphere with 5% CO₂ at 37°C. Identification of cell purity both of primary HEEC and HESC was as previously described [37]. Briefly, cells were seeded on coverslips overnight and fixed with methanol at room temperature for 15 min. Then cells were washed with Phosphate-Buffered Saline (PBS) for 5 min and repeated for 3 times. Cells were incubated with 2 % Triton X-100 in PBS to increase plasmalemma permeability at room temperature for 5 min. Nonspecific binding was blocked by 3 % Bovine Serum Albumin (BSA) for 1 h before incubation with monoclonal anti-cytokeratin actin, or antivimentin actin antibody and incubated overnight at 4°C. The corresponding secondary antibodies were incubated in dark at room temperature for 2 h. Cell structure was visualized by a fluorescence microscope at 490 and 550 nm, respectively. The purity of cells was over 97 % as shown in Fig. S5.

2.6.2. Cell viability assay

To assess the biocompatibility of the CG Cu, UFG Cu and UFG Cu-0.4Mg, the polished samples were sterilized under ultraviolet radiation and incubated in the cell medium solutions of the four cell lines respectively for 24 h. The ratio of the samples' exposedarea to the extraction-medium's volume was 1.25 cm²/mL. The metallic ions' concentrations and the pH values were measured after extraction. The 100 % extracts and extracts diluted to 50 %and 10 % were used in subsequent cell experiments. For cell viability assay, cells cultured in complete medium served as negative controls and positive controls of cell with 10 % dimethyl sulfoxide were used. Cells with a density of 1×10^4 cell/mL were seeded into some 96-well plates to allow attachment. Then the normal culture medium was replaced both with extracted and control media, and further incubated for 1, 3 and 5 days. A cell count kit (CCK-8, Dojindo, Japan) was employed to detect cell viability. 10 µL of CCK-8 solution was added for a 4-hour incubation period with cells. Afterwards, the absorbance value of each plate was measured using a microplate reader (Bio-Rad 680) at 450 nm. Four duplicates were used for each test and the experiment was performed in trip-

2.6.3. Cell cycle test

Cell Cycle and Apoptosis Analysis Kit (Beyotime C1052) was used for cell cycle analysis. HESC were seeded in 12-well plates with a density of 1 \times 10⁶ cells/well. 50 % and 10 % extract were added to the wells and the normal culture medium was the negative control. After 24-hour treatment, cell cycle test was performed according to the instruction of the cell cycle and apoptosis analysis kit. In brief, cells were collected with trypsin, washed in PBS at 4°C, and fixed with 70 % ethanol for at least 1 h. Then the fixed cells could be stored at -20°C for several weeks prior to PI staining and flow cytometric analysis. Before test, cells were centrifuged, washed in PBS and re-suspended in 500 μ L binding buffer at a concentration of 1 \times 10⁶ cells/mL. 25 μ L of PI solution and 10 μ L Rnase A were added and incubated in the dark at 37°C for 30

min. Cells were analyzed using flow cytometry (Becton Dickinson FACSCalibur).

2.6.4. Real-time quantitative PCR

HESC were plated in 6-well culture plates (2×10^6 cells/well) and treated with 10 % extracts. 24 hours later, total RNAs were isolated from cells using Trizol (Invitrogen, USA) following the manufacturer's instruction. The concentration and purity of the RNA from the cells were determined using a NanoDrop 2000C (Thermo Scientific, USA). 0.5 μg isolated cDNAs were used for reverse transcription of mRNA using the PrimeScript RT reagent Kit (TaKaRa Bio, Shiga, Japan). Real time PCR was carried out using the kit (TaKaRa Bio, Shiga, Japan). Primers for inflammation and copper transporter related genes were designed and verified using Primer-Blast from National Centre for Biotechnology Information. The sequences were constructed as listed in Table S1.

The real-time PCR reactions were performed in 48-well optical plates using StepOnePlusTM Real-time PCR system (Applied Biosystems). All experiments were performed in triplicate.

2.7. In vivo studies

2.7.1. Animal treatment

Adult female and male Sprague-Dawley (SD) rats, 10-12 weeks of age (Grade SPF) with a mean mass 250-300 g were obtained from Charles River Laboratories, China. The animals were bred under standard conditions with free access to sterilized drinking water and conventional feed were provided ad libitum. The animals were allowed to acclimatize for 1 week before carrying out the experiment. All protocols for animal care and treatment were approved by the Ethical Committee of National Research Institute for Family Planning.

Sixty sexually mature female SD rats were recruited and randomly divided into four groups: the nonoperation group (n=12) and the sham operation group (n=12), the CG Cu group (n=12), the UFG Cu group (n=12), and UFG Cu-0.4Mg group (n=12). The Cu as the IUD component materials were all shaped in cylindrical rods with the same size: 1 mm in diameter and 10 mm in length. All implants were sterilized under ultraviolet radiation and the corresponding materials were inserted into central portion of the right uterine lumen under pentobarbital anesthesia and aseptic conditions through dorsal incision. After the operation, animals were checked daily to ensure they were in normal condition. Rats in the sham operation group underwent the same operations without insertion of material into the uterine horn.

2.7.2. Monitoring of Cu^{2+} and Mg^{2+} release in serum

Blood samples were collected at days 3, 7, 14, and 28 after insertion from three rats in each group. The blood samples were kept at room temperature for 4 h followed by centrifuge at a speed of 6000 rpm at 4°C for 15 min. The supernatants were collected and stored at -80°C. Before tests, 500 μ L sample in each group were diluted to 1500 μ L with distilled water and mix.

2.7.3. Histological analysis

The rat's uteri were collected at days 3, 7, 14, and 28 after insertion. Uterine tissues were collected from the right uterine horn. Samples were cut into 4 mm in length and fixed immediately in 4 % (w/v) paraformaldehyde (pH 7.2). Then samples were dehydrated in gradient ethanol (75, 80, 85, 95, and 100 %, respectively) and then embedded in paraffin and dissected into 5 μ m sections. Paraffin-embedded tissue sections were deparaffinized and rehydrated in xylene and gradient ethanol (100, 95, 85, 80, and 75% in sequence). Finally, sections were stained with Hematoxylin and Eosin (HE) followed by dehydration and mounted with neutral gummi. The slides were observed under an optical microscope.

2.7.4. Corrosion morphology characterization of the implanted Cu materials

The implanted Cu materials were removed from three animals in each group at days 3, 7, 14, and 28 after insertion, and the corrosion morphology and product on the surface of the Cu materials were characterized using SEM and XRD.

2.7.5. Antifertility experiment

In order to test the contraceptive effectiveness of these Cu materials, 80 sexually mature female SD rats were recruited and randomly divided into four groups: the nonoperation group (n=10) and the sham operation group (n=10), the CG Cu group (n=20), the UFG Cu group (n=20), and UFG Cu-0.4Mg group (n=20). Cu materials were inserted into the right uteri of rats and the sham operation group went through the same surgery procedure without insertion of material into the uteri horn. Rats were allowed to recover for 15 days before mating. The day on which vaginal plug was checked was counted as the day 0.5 of pregnancy. On day 11.5, the animals were sacrificed, and pregnancy outcome was observed via laparotomy and uterotomy. The implanted samples were also taken out and rinsed in distilled water and followed by air-drying, then the corrosion products on the surface were determined by XRD and SEM.

2.8. Statistical analysis

The data in this study are expressed as mean \pm standard deviation. Statistical significance was calculated by non-paired Student's test, and defined as P values less than 0.05.

3. Results

3.1. Microstructures observations of Cu materials

Fig. 1(a-f) shows the grains of Cu materials in EBSD and TEM images. It can be seen from Fig. 1(a) that the grain size of the CG Cu is not uniform ranging from 1 to 20 µm with random grain orientations. The TEM image of Fig. 1(b) did not show the clear grain boundary suggesting the large size of the grain of CG Cu. In Fig. 1(c), the UFG Cu presents much reduced grain size in 300-600 nm after 8-pass ECAP deformation, while the TEM image of UFG Cu in Fig. 1(d) shows more detailed microstructures with the average grain size of 300 nm. The grains do show slight orientation preference. Similarly in Fig. 1(e and f), UFG Cu-0.4Mg alloy possesses ultrafine grains after 8-pass ECAP. The average grain size is 300 nm and grains are slightly preferential oriented along the pressing direction from both EBSD and TEM characterizations. The grain boundary fraction was quite high in UFG Cu and UFG Cu-0.4Mg compared to the CG Cu. Selected Area Electron Diffraction (SAED) was conducted for the single crystals of the Cu materials and the results are shown in Fig. S1. All the SAED patterns can be indexed to [001] which agreed with the f.c.c. Cu (PCPDF #85-1326, a = 0.3615 nm). After the careful calculation of the unit cell parameters including plane angels and the unit cell distance, it can be seen that the angel between {020}, {200} and {220} were 45 $^{\circ}$ for CG Cu matching with the pure Cu. Slight mismatch of the angels (44.9 $^{\circ}$ and 44.8 $^{\circ}$) occurred to UFG Cu, attributed to deviations, however, quite obvious distortion existed in UFG Cu-0.4Mg because of the angels between the planes were 45.3 $^{\circ}$ and 44.9 $^{\circ}$. The unit cell distortion within the UFG Cu-0.4Mg could be owing to the addition of Mg element.

3.2. Long term immersion tests

3.2.1. Cu^{2+} and Mg^{2+} release rate and pH value variation

To compare the metallic ions release behaviors of the three Cu materials, long-term immersion tests in SUF up to 300 days were

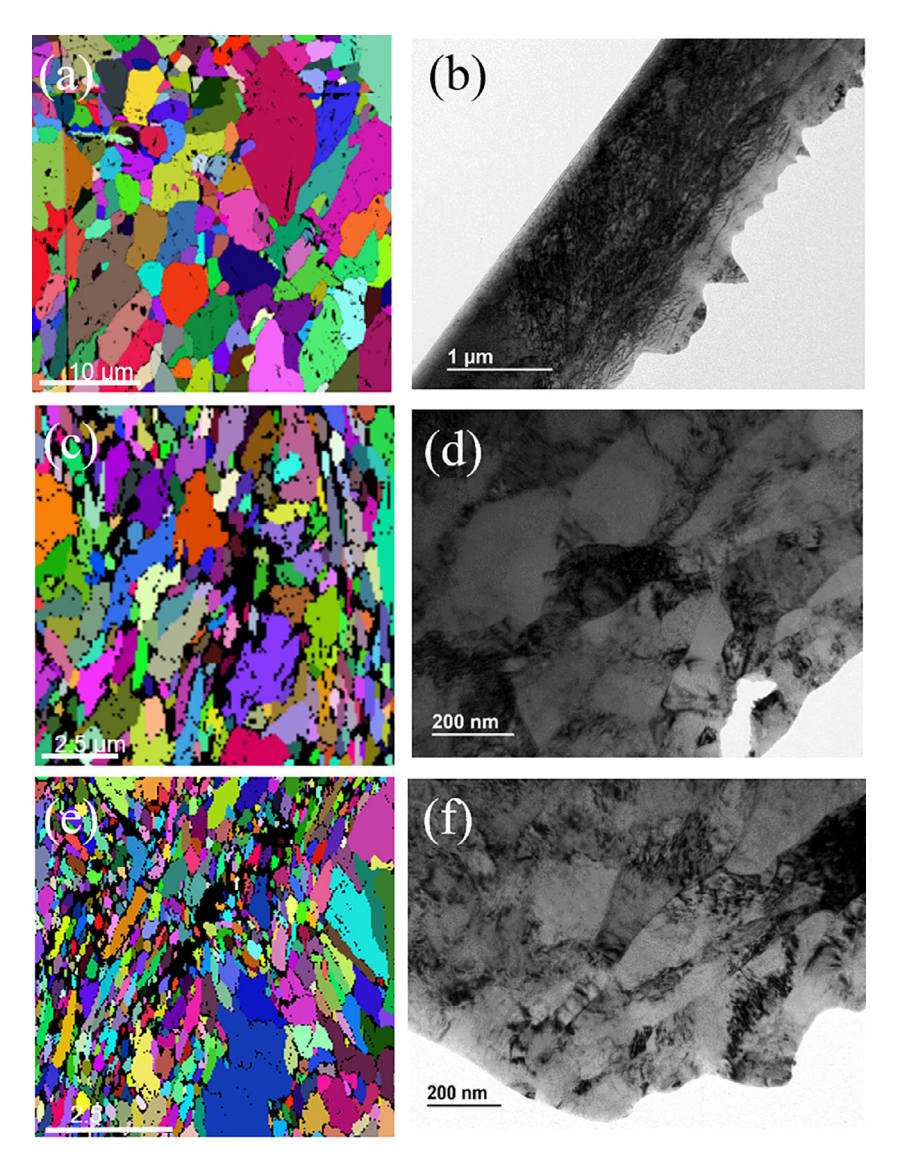


Fig. 1. The microstructures of the Cu materials characterized using EBSD and TEM: CG Cu (a, b), UFG Cu (c, d), and UFG Cu-Mg (e, f).

conducted. The release rate of Cu²⁺ from CG Cu, UFG Cu and UFG Cu-0.4Mg are plotted in Fig. 2(a). All three Cu materials exhibited an initial rapid Cu²⁺ release within the first month followed by the steady release rate after 50-day immersion. The inset figure shows the details of Cu²⁺ release behavior within the first 30 days. The burst release presented within CG Cu was from 163.52 µg/day to 18.30 µg/day from the 1st to 30th day with slight fluctuations from day 5 to day 10. While the release rate of UFG Cu was greatly reduced from 112.34 $\mu g/day$ on the 1st day to 17.44 $\mu g/day$ on 30th day. The release of Cu²⁺ from UFG Cu-0.4Mg on the 1st day was further dropped to 76.63 µg/day. However, the release rate after 30-days' immersion from UFG Cu-0.4Mg was still 15.88 µg/day. It can be observed that the UFG Cu-0.4Mg exhibited the minimized burst release rate of Cu²⁺ owing to the high fraction grain boundary and synergistically, the more electrochemically active Mg addition. The long-term release rate of Cu²⁺ gradually became steady towards to similar level after 50-days' immersion and ended at 0.71, 1.60 and 1.93 μ g/day for CG Cu, UFG Cu and UFG Cu-0.4Mg, respectively. Therefore, both the much-reduced burst release and well-maintained long-term release of Cu^{2+} are achieved from UFG Cu-0.4Mg.

The release rate profile of Mg²⁺ from UFG Cu-0.4Mg immersed in SUF for 300 days is displayed in Fig. 2(b). Corresponding with the Cu²⁺ release, the Mg²⁺ release shows relatively higher rate in the first month and became quite stable after 40-days' immersion. The high release rate of Mg²⁺ in the initial day was along with the burst release of Cu²⁺. The initial release rate at 3.92 µg/day decreased slowly on day 10, then the decreasing tendency was a bit more obvious until day 40. The decreasing tendency for Mg²⁺ is slower than that of the Cu²⁺ for UFG Cu-0.4Mg in SUF within the first 30 days, indicating the preferentially early release of Mg²⁺. The long term Mg²⁺ release rate was kept around 0.8 µg/day. pH values of SUF and corrosion rate were also detected at scheduled timepoint. As shown in Fig. S2. We observed relatively higher pH values of the UFG Cu-0.4Mg group after 20-days' immersion, which could be attributed to the Mg dissolution into the SUF.

3.2.2. Corrosion product, morphology and corrosion rates

The corrosion products analysis of CG Cu, UFG Cu and UFG Cu-0.4Mg after immersed in SUF for different time were characterized using XRD as shown in Fig. S3. Cu_2O was identified as the only corrosion product in all three Cu materials within SUF for up to

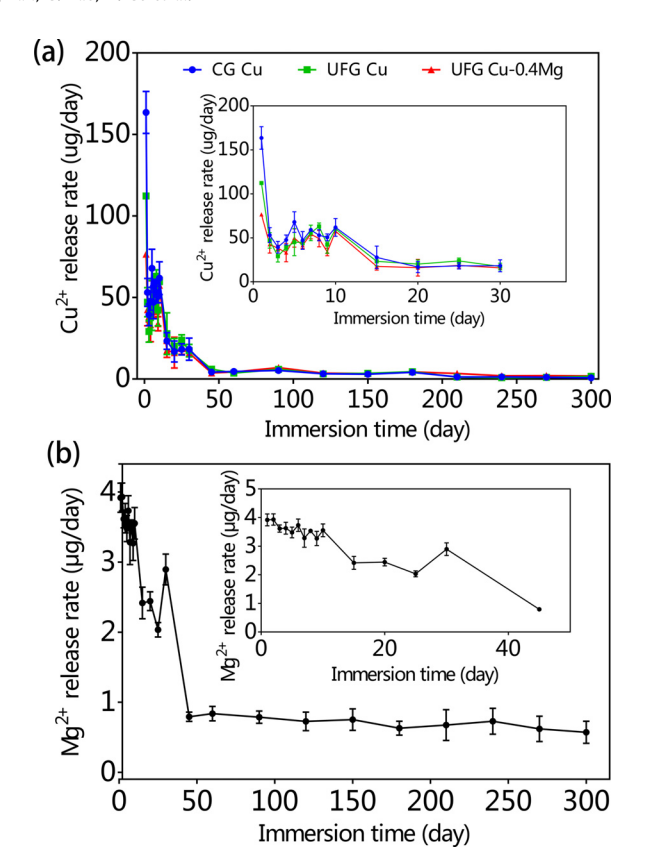


Fig. 2. Long-term Cu^{2+} release rate (a) of CG Cu, UFG Cu and UFG Cu-0.4Mg and Mg^{2+} release rate of UFG Cu-0.4Mg (b) immersed in SUF at 37°C up to 300 days.

Table 1Elemental composition analysis on the *in vitro* corrosion products of the Cu materials using EDS.

Materials	Immersion	Weight concentration (wt.%)					
	time (Days)	Cu	0	С	P	Cl	Ca
CG Cu	10 300	14.4 56.9	85.6 19.7	4.3	- 11.1	2.4	- 5.6
UFG Cu	10 300	34.6 20.2	65.4 54.9	- 3.4	- 13.3	- 4.1	- 4.1
UFG Cu-0.4Mg	10 300	9 18	91 53.8	- 9	- 12	- 3.2	4

300 days. The corrosion product amount increased with the prolonged immersion time in SUF as the relative peak intensities of Cu₂O compare to those of Cu increased gradually. Corrosion product of Mg dissolution was merely found from UFG Cu-0.4Mg. Fig. 3 exhibits the evolution of the corrosion morphology of the CG Cu, UFG Cu and UFG Cu-0.4Mg with the immersion time from 1 to 300 days. After 1-day immersion, the surfaces of all the three Cu materials show newly formed corrosion products along the grinding scratches, corresponding to the burst release of the Cu²⁺ in the first day due to the largely exposed surface areas of Cu materials. After 10 days, it can be seen that a loose layer of corrosion products covered the whole surfaces of the CG Cu, UFG Cu and UFG Cu-0.4Mg. However, in comparison with the CG Cu, both the corrosion product layers on UFG Cu and UFG Cu-0.4Mg are relatively uniform and dense. EDS analysis (Table 1) confirmed the composition of the corrosion products presenting only Cu and O elements for all Cu materials in SUF after 10-days' immersion. During the 30-day immersion, a more compact Cu2O layer formed as the directly contact corrosion layer of the Cu materials surfaces, which could be attributed to the obvious decrease in the release rate of

metal ions from 15 to 30 days (Fig. 2(a)). There were some aggregated deposits formed on the CG Cu surface but not on the UFG Cu and UFG Cu-0.4Mg surfaces, suggesting non-uniform corrosion product and higher Cu²⁺ release in CG Cu within the first month than in UFG Cu and UFG Cu-0.4Mg. Even more aggregated deposits in large size appeared on the surfaces of the CG Cu for 60-days' immersion. The second deposit layer was formed as well on the UFG Cu and UFG Cu-0.4Mg surface after 60 days, the size of aggregates was much smaller and uniform. After 150-days' immersion, CG Cu showed a thicker and denser layer of secondary corrosion product, while porous and fluffy corrosion layers both on the UFG Cu and UFG Cu-0.4Mg surfaces, which could be helpful for the relatively higher Cu2+ release around 150 days [21]. It is worth noting that some small air voids were found from the uniform corrosion product layer on the UFG Cu-0.4Mg surface. The CG Cu surface in SUF after 300-day immersion showed the formation of another corrosion layer with big chunk corrosion products. While larger and more deposits were formed uniformly on the UFG Cu surfaces, the fluffy aggregates became compacted solids. On UFG Cu-0.4Mg surfaces, uniform corrosion product layer with air voids were formed and the observation exhibits porous and fluffy corrosion products observed at higher magnification. EDS analysis showed that the corrosion products mainly composed of Cu, O, Ca, P, Cl, and C (shown in Table 1) after 300-day immersion in SUF. Mg-containing products was hardly found in the corrosion products on UFG Cu-0.4Mg surface.

The corrosion rates calculated using the weight loss of Cu materials according to Eq. (1) after immersed in SUF up to 300 days (Fig. S4) present much lower corrosion rate of UFG Cu-0.4Mg comparing both with CG Cu and UFG Cu. Especially the first day release, without effect of corrosion product on the Cu materials surfaces, the preferentially early release of Mg²⁺ successfully reduced the Cu²⁺ release. After 10-days' immersion, the corrosion products formed and covered the whole surface, which greatly reduced the metallic ions release, although UFG Cu-0.4Mg still show lower corrosion rates.

3.3. Electrochemical test

Fig. 4 displays the electrochemical polarization curves of Cu materials in SUF. The corrosion parameters including corrosion current density (i_{corr}) and the corrosion potential (E_{corr}) were obtained using Tafel extrapolation method as listed in Table 2. The general shapes of all the polarization curves are alike, and the corrosion rates were consistent with the long-time immersion test. The variations in corrosion current are principally associated with the variations in cathodic currents. It can be seen that the cathodic current densities of CG Cu were higher than those of UFG Cu and UFG Cu-0.4Mg in SUF. It could also be observed that when cathodic polarization potentials exceeded -0.52 V_{SCE} , the current densities of UFG Cu-0.4Mg were higher than those of UFG Cu until -0.31 V_{SCF}. This was because ionization of Mg augmented the current densities and the evolution of hydrogen [38] according to the following reaction Eqs. (2)–((4)) which was in line with the small air voids formed on the surface of UFG Cu-0.4Mg immersed in the SUF as shown in Fig. 3. When the cathodic polarization potentials were above -0.31 V_{SCE} , UFG Cu-0.4Mg showed the lowest current density. The anodic Tafel slope of the three materials were similar as the obvious passivity breakdown of UFG Cu and CG Cu could be observed. The passivation process was related to the formation of a layer of Cu₂O. The anodic reaction was the copper dissolution shown in Eq. (5) since the neutral SUF containing chloride ions involved the cathodic reduction of oxygen (Eq. (2)), and the anodic reaction was the copper dissolution shown in Eq. (5). The presence of CuCl2- at the metal surface leads to a hydrolysis reaction and the formation of Cu₂O film [39] which was also detected in vitro

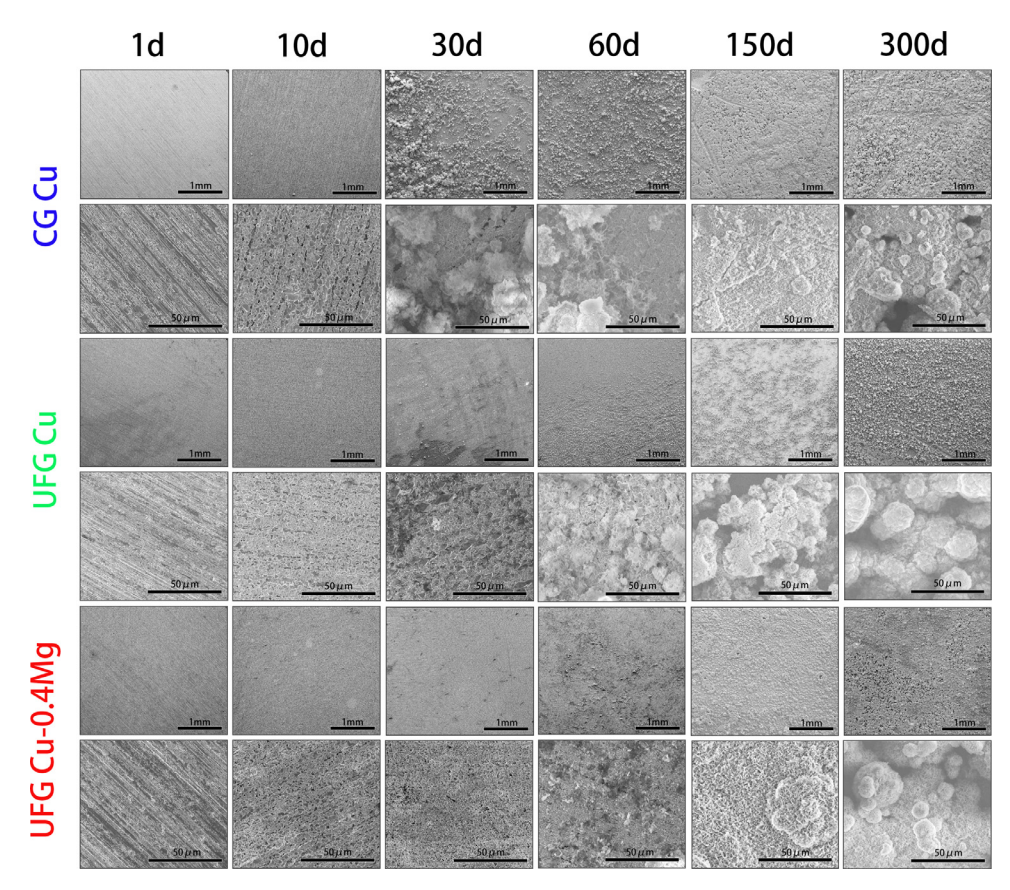


Fig. 3. Corrosion morphology observation of CG Cu, UFG Cu and UFG Cu-0.4Mg after immersion in SUF for 1, 10, 30, 60, 150 and 300 days.

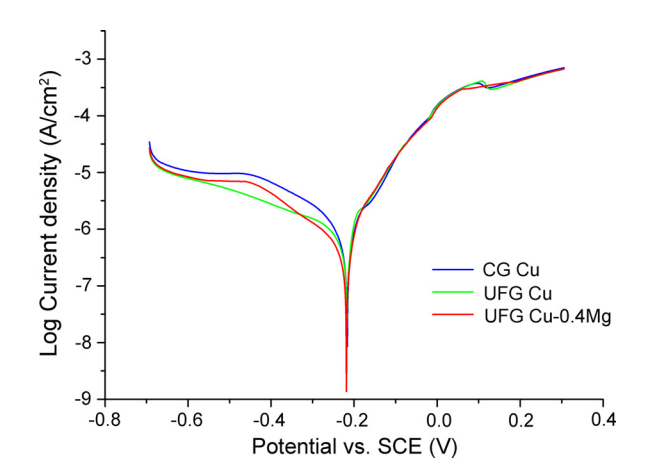


Fig. 4. The electrochemical polarization curves of the three Cu materials in SUF.

immersion test and generates partially the soluble ions in solution, thus the Cu_2O film hinder the effective release of ionic copper of the two Cu materials compared with the Cu alloy in the long-term in *vitro* test. Therefore, the reduction of the grain size and increase

of the grain boundary fraction on the corrosion surface of the Cu materials significantly enhanced the corrosion resistance in SUF. It also can be seen from Table 2 that the addition of Mg element into the Cu greatly increased the corrosion resistance of UFG Cu-0.4Mg in comparison with UFG Cu.

$$2H_2O + O_2 + 4e^- \rightarrow 4OH^-$$
 (2)

$$Mg \rightarrow Mg^{2+} + 2e^{-} \tag{3}$$

$$Mg^{2+} + 2H_2O \rightarrow Mg^{2+} + 2OH^- + H_2$$
 (4)

$$Cu + 2Cl^{-} \rightarrow CuCl_{2}^{-} + e^{-}$$
 (5)

$$2CuCl_2^- + H_2O \rightarrow Cu_2O + 2H^+ + 4Cl^-$$
 (6)

3.4. In vitro tests

3.4.1. In vitro cytocompatibility tests

Four different cell lines, including three cells related to human uterus (HUVES, HEEC and HESC) and one typical cell toxicity assessment cell line (murine fibroblast cells, L-929) were used to investigate the cytocompatibility of the three Cu materials. Identification of the HEEC and HESC were performed by immunofluorescence (IFC) as shown in Fig. S5 and the purity of both cell lines met

Table 2 Corrosion potential (E_{corr}), corrosion current density (i_{corr}), electrochemical transfer coefficients and corrosion rate of CG Cu, UFG Cu and UFG Cu-0.4Mg obtained from electrochemical tests.

Materials	E_{corr}/V vs. SCE	i _{corr} (A/cm ²)	β a (mV/dec)	β c (mV/dec)	Corrosion rate (mm/year)
CG Cu UFG Cu	$\begin{array}{c} 0.208 \pm 0.002 \\ 0.21 + 0.01 \end{array}$	$4.471 \pm 0.071 \times 10$ $2.689 + 0.064 \times 10$	242.7 197.7	-91.8 -95	$\begin{array}{c} 0.052 \pm 0.001 \\ 0.031 + 0.001 \end{array}$
UFG Cu-0.4Mg	0.215 ± 0.008	$2.305 \pm 0.054 \times 10$ $2.305 \pm 0.051 \times 10$	192.4	-86.6	0.027 ± 0.001

Table 3 Cu^{2+} and Mg^{2+} concentration in culture media both before and after incubating with CG Cu, UFG Cu and UFG Cu-0.4Mg for 24h.

Cell culture medium Material	DMEM		DMEM-F12		
	Cu ²⁺ (mM)	Mg ²⁺ (mM)	Cu ²⁺ (mM)	Mg ²⁺ (mM)	
NC CG Cu UFG Cu UFG Cu-0.4Mg	$/$ 4.851 ± 0.199 3.682 ± 0.291 2.232 ± 0.203	0.806 ± 0.012 0.816 ± 0.009 0.816 ± 0.014 0.877 ± 0.008	5.2×10^{-6} 3.273 ± 0.164 2.411 ± 0.19 1.835 ± 0.068	$\begin{array}{c} 0.71 \pm 0.005 \\ 0.717 \pm 0.004 \\ 0.720 \pm 0.004 \\ 0.73 \pm 0.007 \end{array}$	

Table 4 Cell cycle assay of HESC cultured in 50 % and 10 % extraction media (mean \pm SD). + Proliferation index (PI) represents the ratio of between the S and the G2/M phases in the whole cell cycle (i.e., PI = (S + G2/M) / (G0 / G1 + S + G2/M), cell proliferation ratio = PI \times 100 %).

Groups	G0/G1(%)	S (%)	G2/M (%)	PI + (%)
NC	61.8±1.05	17.08±1.34	21.12±0.28	38.20±1.05
10%Cu	59.26 ± 0.8	17.41 ± 2.53	23.32 ± 3.32	40.74±0.79#
10%UFG-Cu	58.69 ± 0.01	18.38 ± 0.94	22.94 ± 0.95	41.32±0.01#
10%UFG-Cu0.4Mg	51.48 ± 0.66	21.43 ± 2.25	27.10 ± 1.6	48.53±0.66**
50%Cu	82.5 ± 0.7	10.19±0.86**	7.31 ± 0.16	17.5±0.7*
50%UFG-Cu	80.82 ± 0.33	5.53±0.37**	13.66 ± 0.71	19.19±0.33*
50%UFG-Cu0.4Mg	78.78 ± 2.93	11.88±1.03**	9.52 ± 1.65	21.36±2.73*

^{*} $P \le 0.05$ and ** $P \le 0.01$ when compared with the negative group.

the requirements of experiment. The concentrations of the Cu²⁺ and Mg²⁺ in the extracts were quantified and listed in Table 3 after the Cu materials were incubated with the cell culture medium for 24 h. The Cu²⁺ concentration for CG Cu, UFG Cu and UFG Cu-0.4Mg decreased in both mediums showing the less burst release of Cu²⁺ from UFG Cu-0.4Mg. On the other hand, the Mg²⁺ concentration can be found higher from UFG Cu extract because Mg²⁺ was pre-existed in both media. Moreover, the pH values of the culture media were measured both before and after the incubation of Cu materials as shown in Fig. S6. The pH values of medium increased from 7.5 to 8 from the reaction of the Cu materials with culture media, release of the metallic ions and probably consummation of the medium nutrition.

The calculated CCK8 results based on Figs. 5 and S7 display very severe cell toxicity of all the four cell lines from both the 100 % and 50 % extracts of all three Cu materials. The cell viability of the four cell lines presented significant difference (p < 0.05) between the negative control and the 100 % and 50 % extracts of all three Cu materials for different culture time. The cell viability also decreased sharply with time. CG Cu appeared to be more toxic than the UFG Cu and UFG Cu-0.4Mg to all the cells. To further investigate the long-term effect of Cu^{2+} from CG Cu, UFG Cu and UFG Cu-0.4Mg on cell viability, 10 % extracts were used as well (Fig. 5). 10 % extracts of UFG Cu and UFG Cu-0.4Mg showed almost no toxicity to the four cell lines on the first day while the 10 % extract of CG Cu exhibited relatively low cell viability to HEECs, HESCs and L-929 cells for the first day culture. For the 3- and 5-days' culture, cell viability decreased dramatically for CG Cu while the cell viability for UFG Cu and UFG Cu-0.4Mg decreased slightly, especially the UFG Cu-0.4Mg. It is worth noting that UFG Cu-0.4Mg displayed significant effect on the proliferation of HESC cells (Fig. 5b) with a cell viability of 111 %. The cell viability tests show the elevated cytocompatibility of UFG Cu-0.4Mg with the addition of Mg compared with UFG Cu and CG Cu.

3.4.2. Cell cycle assay

Cell cycle analysis was performed to quantitatively characterize the toxicity of Cu materials to HESCs. The proliferation phases of the HESC cells after cultured in 10 % and 50 % extract of the Cu materials for 24 h were recorded and the proliferation index (PI) was calculated and shown in Table 4. Comparing with the negative control, the HESCs in S phase dropped significantly after the HESCs were incubated within 50 % extracts for 24 h while the S phase increased when the HESCs were incubated in 10 % extracts of the three Cu materials. G2/M phase percentage and the PI values showed a similar trend to the S phase for the three Cu materials. It can be observed that UFG Cu-0.4Mg exhibited the best cytocompatibility to the HESCs with high percentages of S and G2/M phases as well as PI values in both 10 % and 50 % extracts. The detailed analysis on the cell cycle for the three Cu materials displayed consistent results with the cell cytotoxicity evaluation.

3.4.3. Quantitative real-time PCR analysis

After the HESCs were cultured in the 10 % extract of the three Cu materials, genes related to inflammation (Human IL-1 β , Human IL-6, and Human IL-8) and the copper ions transport (Human ATP7A and Human CTR1) were quantified using real-time PCR analysis. The results are shown in Fig. 6. The relative expressions of IL-1 β , IL-6 and IL-8 (Fig. 6(a)) from the HESCs in CG Cu and UFG Cu extracts were obviously higher than that from the UFGCu-0.4Mg extract which was at similar expression level with the control group. Thus, UFG Cu-0.4Mg presented lowest inflammation response which was indicating much improved cytocompatibility with the addition of the Mg alloy element into UFG Cu. Copper homeostasis in mammalian cells are under the control of copper transport proteins such as copper importer CTR1 (copper transporter 1) and exporter ATP7A (copper-transporting Ptype ATPase/Menkes ATPase). CRT1 usually uptakes and transports into cells for the synthesis of copper-dependent enzymes through three different metallochaperone-mediated copper delivery pathways. The relative expression of CRT1 in the HESCs was much higher from both the CG Cu and UFG Cu extracts than that from the UFG Cu-0.4Mg extract and negative control group (shown in Fig. 6(b)) indicating the higher copper homeostasis in HESCs from larger amount of copper ion from the extracts. Moreover, ATP7A plays an important role in excess copper ion exporting. The ATP7A was significantly increased both in the UFG Cu and CG Cu when compared with the control and UFG Cu-0.4Mg. These results together demonstrated that the addition of Mg into the UFG Cu re-

[#]P≤0.05 when compared with the UFG Cu-0.4Mg group.

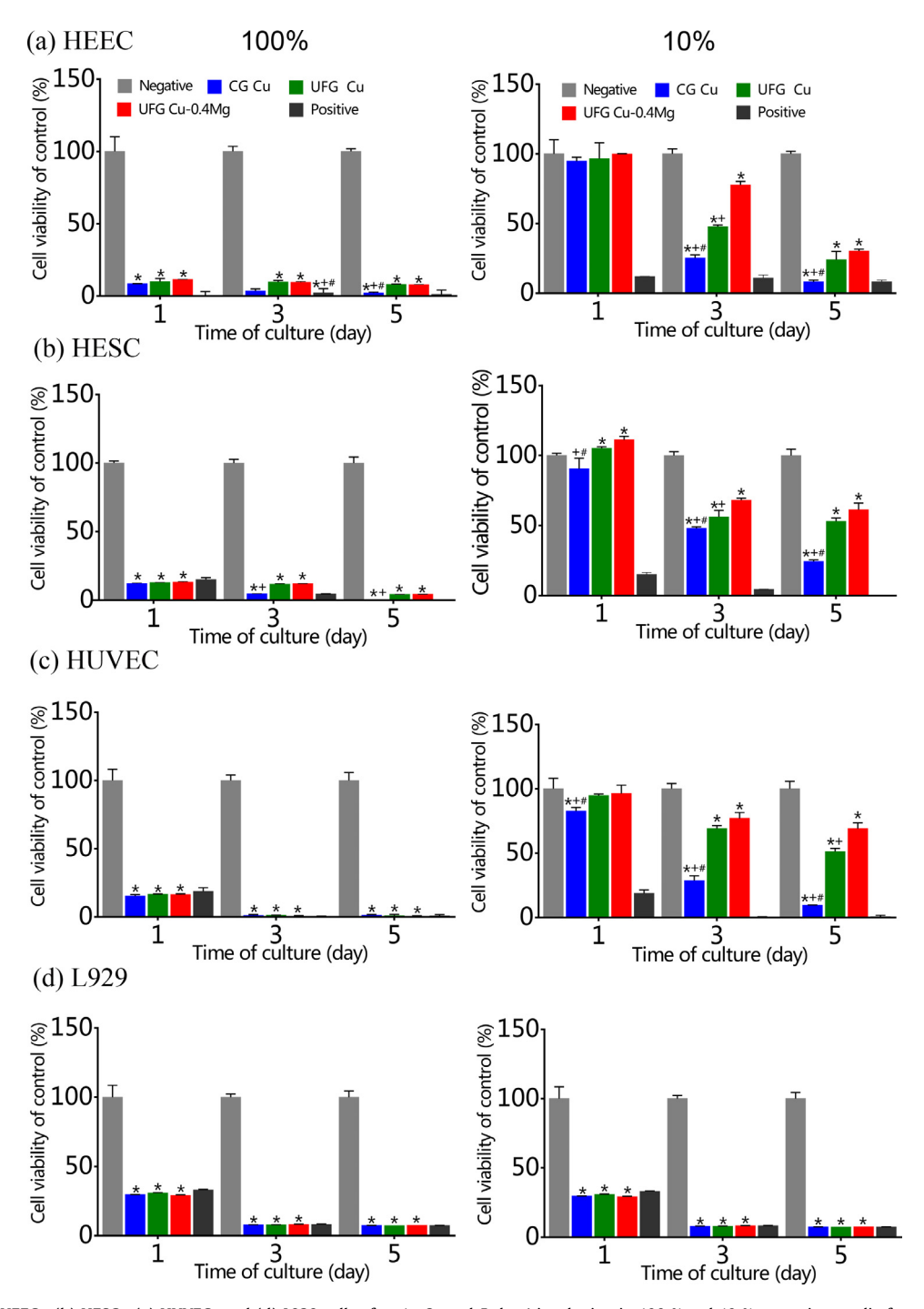


Fig. 5. Viability of (a) HEECs, (b) HESCs, (c) HUVECs and (d) L929 cells after 1-, 3- and 5-days' incubation in 100 % and 10 % extraction media from the CG Cu, UFG Cu and UFG Cu-0.4Mg. $^*P \le 0.05$ when compared with the uFG Cu-0.4Mg group; $^\#P \le 0.05$ when compared with the UFG Cu group.

sulted in not only a significant reduction in inflammation reaction but also extracellular Cu^{2+} concentration.

3.5. In vivo implantation test

3.5.1. Histological evaluation

The morphological evolution of the uterus tissues was dynamically observed at different time points after the Cu materials' implantation into the rats' uteri. Histologic examination of endometrial tissue which directly contacted with the implanted materials is revealed in Fig. 7. The morphological evolution of the sham operation was displayed in Fig. S8. Sight inflammatory response was

observed indicating the surgery operation had little influence. An acute inflammatory response had occurred at the contact site after 3-days' implantation of all three Cu materials. The overview of the uterus tissues was shown in the insets and the red square labelled area corresponded to each histopathology images. Using the control group as a reference, the irregular morphology was found for the tissue at the contact area of uterus with CG Cu, UFG Cu and UFG Cu-0.4Mg. Most endometrial epithelial cells disappeared, glands number decreased, and neutrophilic granulocytes exude from the uterine tissue into the uterine cavity as pointed by red arrows in Fig. 7. Moreover, extensive vacuolation of epithelium cells was observed in CG Cu group suggesting severe damage. Con-

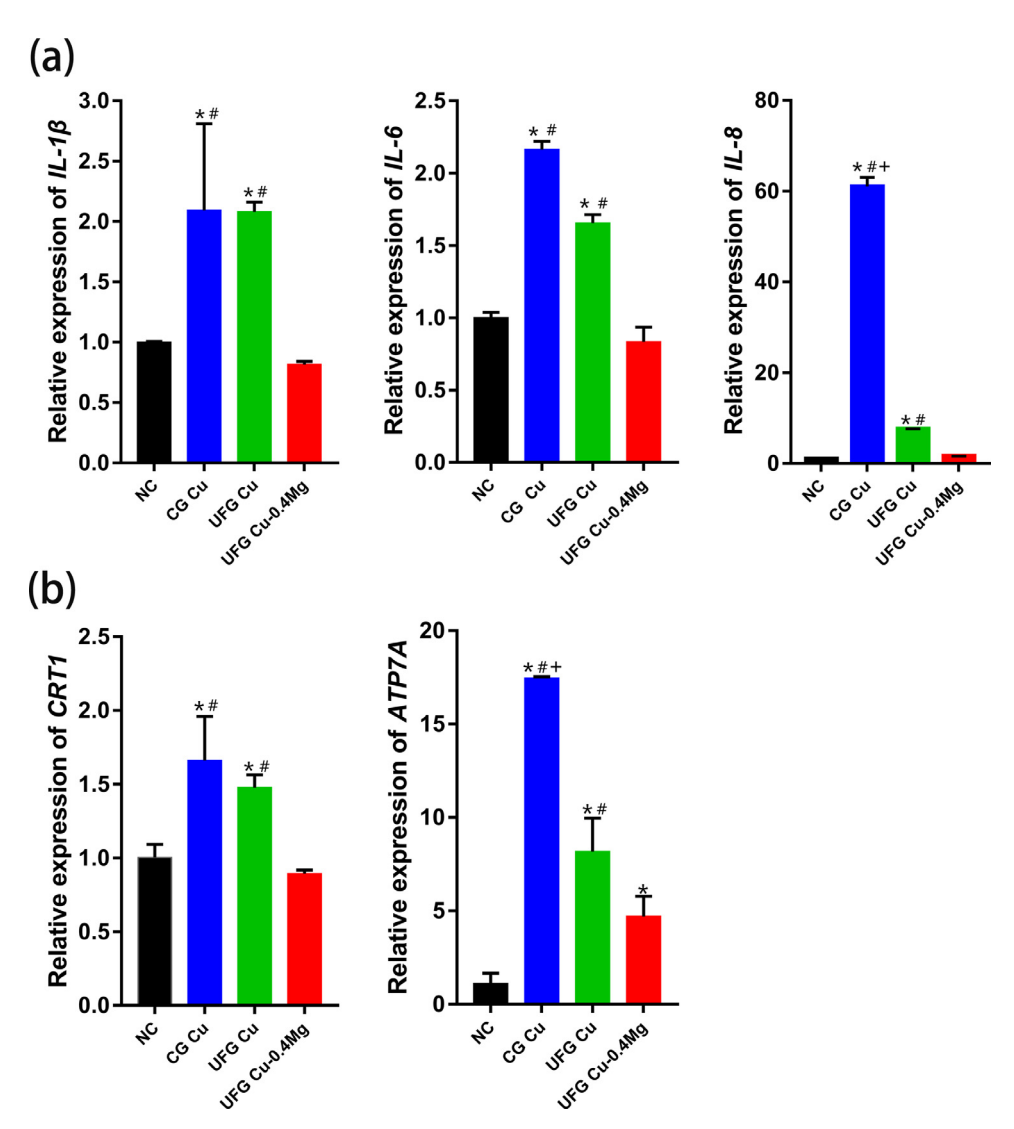


Fig. 6. Inflammation related genes IL-1β, IL-6 and IL-8 expression (a) and copper transporter related genes CRT1, ATP7A and ATP7B in HESCs in CG Cu, UFG Cu-0.4Mg extraction media diluted to 10 %. *P≤0.05 when compared with the uFG Cu-0.4Mg group; *P≤0.05 when compared with the UFG Cu group.

tinuous damage was visible in the uterus tissues after 7-days' implantation of CG Cu. More lymphocytes infiltrated into stroma and epithelial fibrosis appeared. Meanwhile, increased microvessles (as pointed by yellow arrows in Fig. 7) in subepithelial stroma were presented in the tissue contacted with UFG Cu indicating the intensified inflammation responds. For the uterus tissues contacted with UFG Cu-0.4Mg, only a small number of lymphocytes were observed in uterine stroma. The squamous metaplasia phenomenon (as pointed by green arrows in Fig. 7) of the uterine endothelial cells, a protective mechanism formed after progressive inflammation [40], was found in the tissues contacted with both CG Cu and UFG Cu group for 14- and 28-days' implantation. However, compromised inflammatory reaction and recovery of endometrial epithelium were observed in the uterus tissue contacted with UFG Cu-0.4Mg for 14-days' implantation. Moreover, the structure of endometrial cells and number of glands were close to normal with only slight inflammatory reaction at day 28.

We also investigated the response of the uterine tissue adjacent to the Cu materials implants. Fig. 8 displays the uterus tissue morphologies after the Cu materials were implanted into the rats' uteri for different time. The insets in each histopathology images are the full view of the tissue slice while the red square area corresponded to the high magnification view. The morphology of uterus tissues

showed the intact uterine structure and no observable difference among the tissues during the implantation time. No morphologic changes of tissues could be found in the short implantation time within 3 and 7 days. However, severe inflammatory reaction in stroma in the later stage (14 days) could be observed in the tissue adjacent to CG Cu implantation comparing to the mild reactions in the tissues adjacent to UFG Cu and UFG Cu-0.4Mg materials. Moreover, interstitial fibrosis and vascular hyperplasia in superficial muscular layer also occurred in the uterine tissue adjacent to CG Cu after 28 days owing to the long-term inflammatory stimulation. Together with the histomorphology analysis of the uterus by histologic examination, it can be seen that severe inflammatory response could be induced to both the contacted uterus tissues and adjacent tissues from CG Cu and UFG Cu during the implantation while UFG Cu-0.4Mg exhibited much improved histocompatibility with moderate inflammation reaction because of the addition of Mg element.

3.5.2. Cu^{2+} and Mg^{2+} concentration in serum

High level Cu^{2+} in uterine fluid would affect the concentration of Cu^{2+} in blood, it is essential to assess the concentrations of metal ions in serum induced from the implanted Cu materials in uterus. The concentrations of Cu^{2+} and Mg^{2+} in blood were mea-

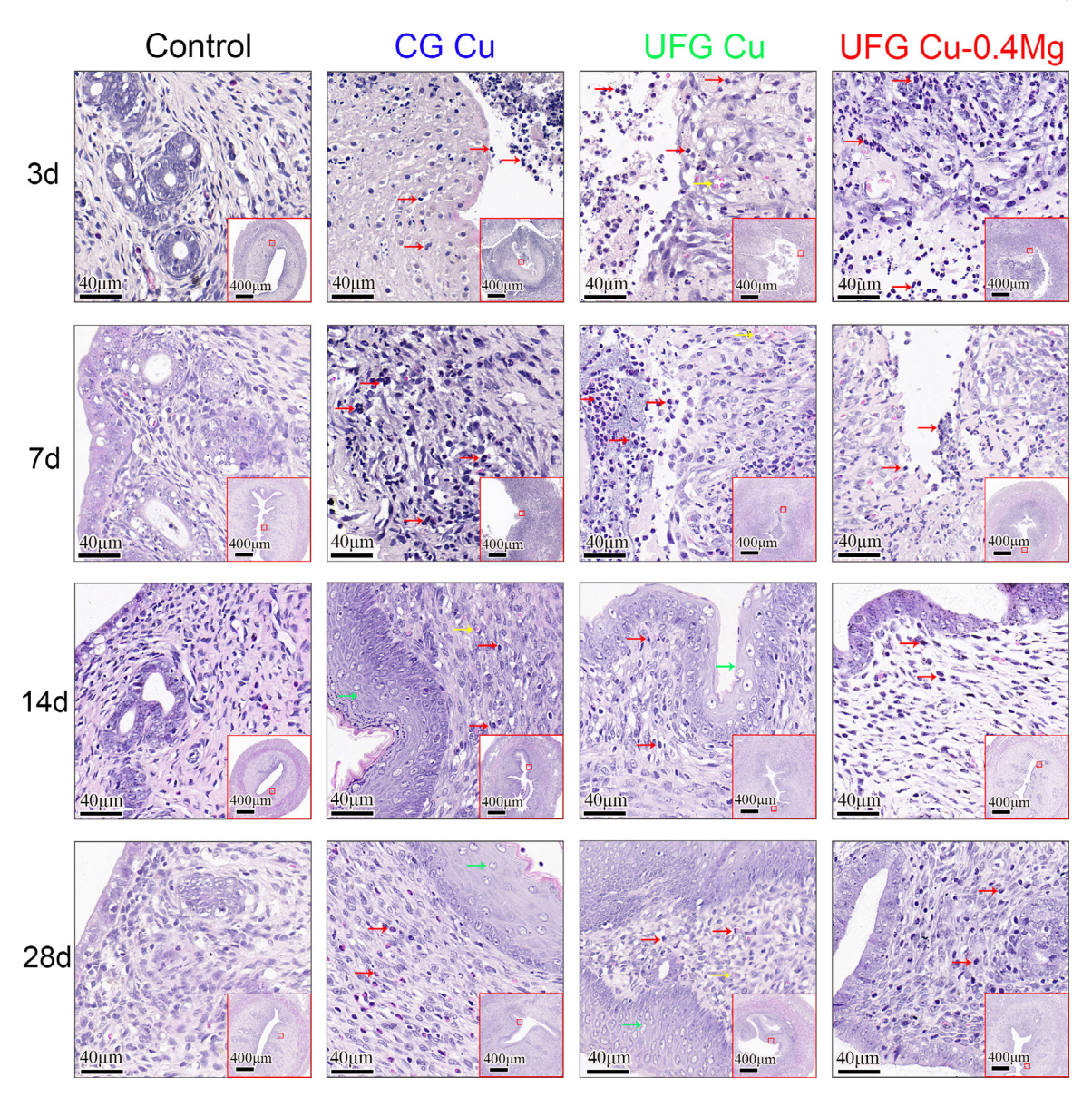


Fig. 7. Histopathology images of endometrium for the control rats and the CG Cu, UFG Cu and UFG Cu-0.4Mg inserted rats obtained from the tissue samples collected at different timepoints. Red arrows point the neutrophils, green arrows for the squamous metaplasia phenomenon of the uterine endothelial cells and yellow arrows for the micro vessels. (For interpretation of the references to the color in this figure legend, the reader is referred to the web version of this article.)

sured using ICP-MS after the Cu materials implanted into the rats' uteri and the results are shown in Fig. S9. The statistic Cu²⁺ concentration in blood after 3-days' implantation of the Cu materials was significantly different from the control group, ~1.5 times higher, indicating the burst release of Cu²⁺ in the first 3 days from the Cu materials in uterine directly affected the Cu²⁺ level in the blood. While the Cu²⁺ concentrations in blood showed no obvious difference among the three Cu materials. After 7-days' implantation, the concentration in the CG Cu and UFG Cu were still higher than that of the control group with significant differences. However, the Cu²⁺ concentration in blood for the rats bearing the UFG Cu-0.4Mg exhibited no significant difference with the control group. The Cu²⁺ concentration in blood for the rats bearing the Cu materials gradually decreased to the level of the control group after 14- and 28-days' implantation, suggesting there was no more influences on the Cu^{2+} level in blood from the Cu^{2+} in uterine. For the Mg²⁺ concentration measured in the blood of rats bearing Cu materials in uterine (Fig. S9(b)), no significant difference among the samples and control group was observed in the 28-days' implantation.

3.6. Antifertility tests

To determine the contraceptive capability of the Cu materials, the antifertility experiment was performed using the rat model and the results are summarized in Table 5 and normal embryo could be detected in all contralateral uterine horns in the sham operation group (Table S3). No embryos were observed in the uterine horns where the Cu materials were implanted, while 8 normal embryos on average were found in the contralateral uterine horns of all the rats bearing with Cu material as well as control group. Antifertility rates for the rats bearing with the three Cu materials were all 100 %, suggesting that Mg addition did not attenuate the antifertility efficacy of Cu materials.

3.7. Corrosion products and corrosion morphology of the implanted Cu materials

3.7.1. Corrosion morphology

The corrosion morphology of the Cu materials was characterized using SEM after they were implanted into the uteri of rats for

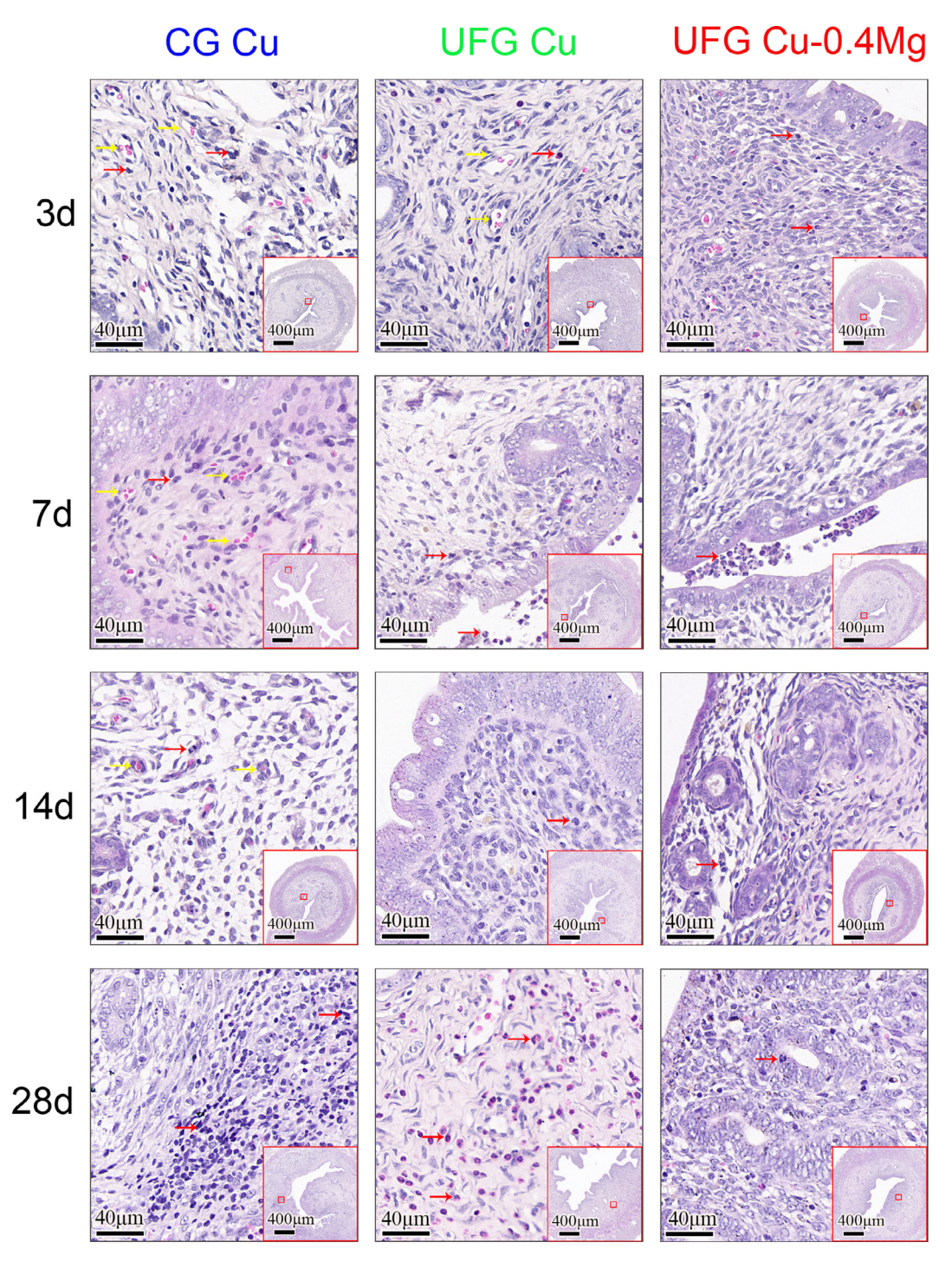


Fig. 8. Histopathology images of endometrium next to the Cu materials implanted site. Red arrows point the neutrophils and yellow arrows for the micro vessels. (For interpretation of the references to the color in this figure legend, the reader is referred to the web version of this article.)

Table 5 Antifertility results of the Cu materials.

Group	п	Number of embryos in material-bearing uterine horn	Number of embryos in contralateral uterine horn	Number of pregnant animals	Antifertility rate (%)
CG Cu	20	0	8.4±1.6	0	100*
UFG Cu	20	0	8±2	0	100*
UFG Cu-0.4Mg	20	0	7.9 ± 1.9	0	100*
NC	10	$7.4{\pm}0.5$	7.8±1.3	10	0

^{*} $P \le 0.05$ when compared with the negative group.

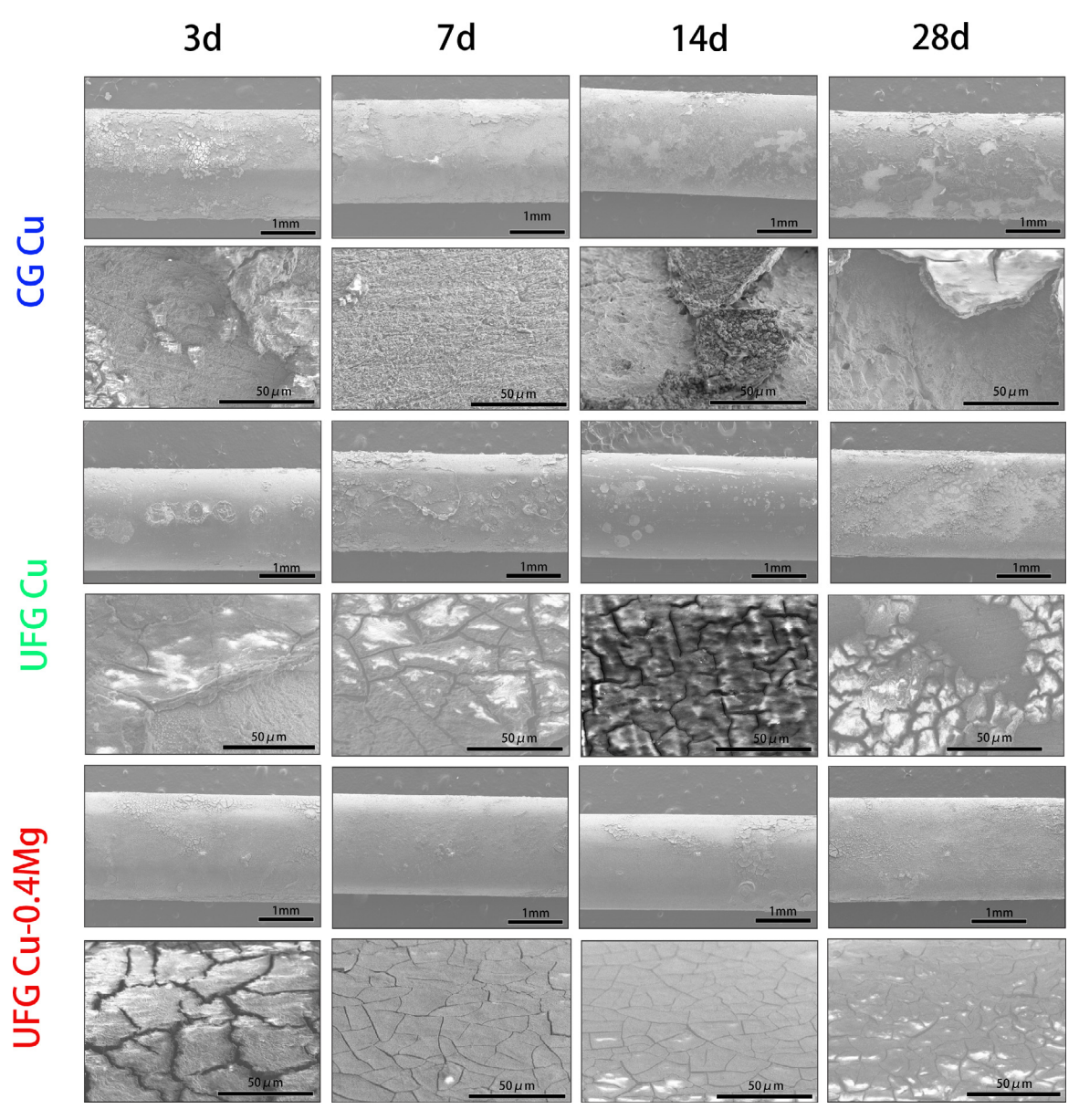


Fig. 9. Corrosion morphology observation of the CG Cu, UFG Cu and UFG Cu-0.4Mg after implanted in uterus for 3, 7, 14 and 28 days.

3, 7, 14 and 28 days and the results were shown in Fig. 9. It can be observed that the corrosion product layer was rapidly formed since 3-days' insertion and the surfaces of the all three Cu rods became rougher with longer time, however, when comparing the three Cu rods, UFG Cu-0.4Mg showed a much smoother corrosion surface than the CG Cu and UFG Cu thorough the 28 days. A second layer of corrosion products was formed on CG Cu and UFG Cu surfaces for 7-days' implantation and on UFG Cu-0.4Mg for 14-days' insertion. The crack and peeling of the corrosion layer on CG Cu rod appeared on the 14th day and became very severe on the 28th day. Both UFG Cu and UFG Cu-0.4Mg rods did not present local peelings from its surfaces.

3.7.2. Corrosion products composition

It can be observed that thick layers of corrosion product formed on Cu rods surfaces within the first 3-days' implantation. The elemental compositions of the corrosion product at the two spots were analyzed using EDS, respectively. Similar trend in the detailed results can be found for all three Cu materials as shown in Fig. S10. The inner layer of the corrosion products presented high percent-

age of Cu and O and very low other elements, such as C, S, and N. While on the outer layer of the corrosion products, the percentage of Cu and O decreased sharply and the atomic percentage of C, N, O and S increased a lot. After 14-days' implantation, it could be easily found in Fig. S10(a) for CG Cu that most of the corrosion products on the CG Cu surface cracked and peeled off. In Fig. S10(b), Cu composition was 100 % in the labelled C1 zone where inner pure Cu was exposed after the corrosion product fell off. This phenomenon could be attributed to the large grains with low fraction of grain boundary and the discrete distribution of the corrosion products on the surface. Therefore, it may lead to a second time of copper corrosion and burst release *in vivo*. For UFG Cu and UFGCu-0.4Mg, there was no bare Cu surfaces exposed due to the nanoscale grains and high proportion and evenly distributed the grain boundary to hold the corrosion product layer.

The XRD profiles in Fig. S11 shows the phase constitution of the corrosion products on the surface of the Cu materials after implanted in rats for different time. The evolution of corrosion products was more obvious for UFG Cu-0.4Mg with implantation time. It can be seen from Fig. S11 that there was a little Cu₂O

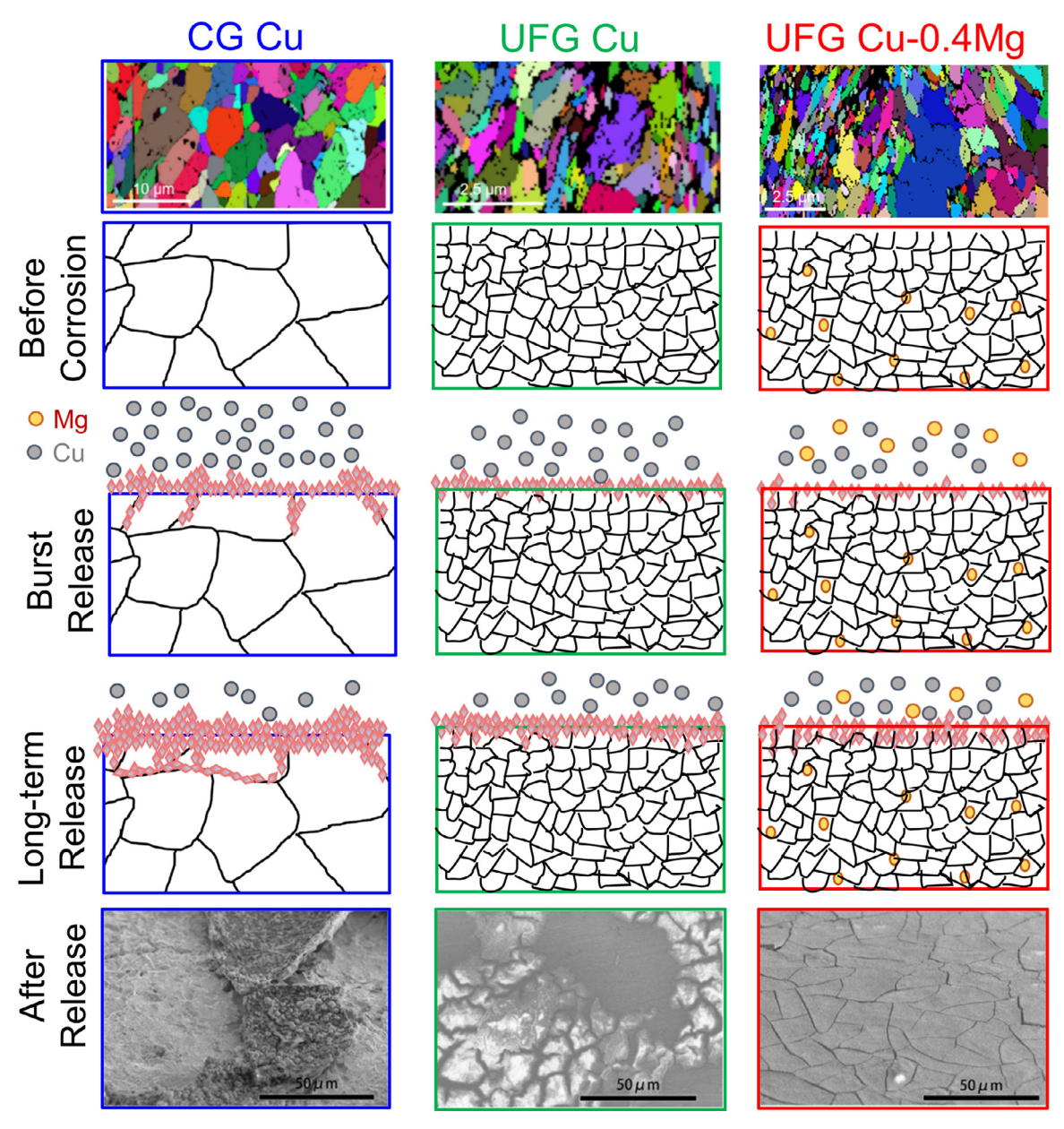


Fig. 10. The illustration of the corrosion process and Cu^{2+} release of CG Cu, UFG Cu and UFG Cu-0.4Mg in SUF.

and main Cu presenting in UFG Cu-0.4Mg with 3-days' implantation time, corresponding to the least burst release at the beginning of implantation. After 7 days, the Cu peaks reduced and Cu₂O peaks increased. This tendency of Cu peaks decreasing and Cu₂O peak increasing continued with implantation time, demonstrating the corrosion product layer increased. In contrast, both the CG Cu and UFG Cu presented all the corrosion products including Cu₂O, Cu₅, Cu₂S and Cu substrate within 3-days' implantation. With the increase of implantation time, Cu₂O increased first and then the other products increased much more in the later implantation time. These results together indicated that UFG Cu-0.4Mg possessed smoother corrosion surface and relative less corrosion products deposition, which corresponds the lower foreign body reaction from Cu materials in the uteri while high contraceptive efficacy was maintained.

4. Discussion

After the systematical investigations and comparisons, the bulk copper with ultrafine grained structures and a small proportion of Mg element exhibited the much-suppressed burst release of Cu²⁺ both in *in vitro* and *in vivo* environments at the initial stage but also presented relatively high long-term Cu²⁺ release in the later stage of the immersion. Moreover, an enhanced *in vitro* cytocompatibility and decreased *in vivo* inflammatory reaction were achieved using UFG Cu-0.4Mg while high antifertility efficacy was well maintained. The UFG Cu-0.4Mg alloy is highly potential to be a new active material for Cu-IUD. With bioactive element alloying, the UFG Cu-0.4Mg preserved the advantages of UFG Cu [21] and manifested much lower Cu²⁺ burst release and higher biocompatibility. The illustration of the Cu²⁺ release of the three Cu materials is shown in Fig. 10.

The mechanism for the effective inhibition of the Cu²⁺ burst release from the UFG Cu-0.4Mg could be attributed to the incorporation of relatively active Mg into the UFG Cu. When the bare Cu materials were immersed in the SUF or implanted into the rat uterus, the large exposed surface areas in fresh solution induced the burst release of Cu²⁺. Compared to the CG Cu, UFG Cu possesses much higher fraction of uniform distributed grain boundaries due to the dramatically reduced grain size of 200~300 nm,

which would reduce the free energy and potential difference between anodic sites (grain boundaries) and cathodic sites (grain interiors) and decrease both local corrosion and the cathodic current. Furthermore, the high fraction of grain boundaries of UFG Cu could facilitate the rapid formation of a homogeneous and dense Cu₂O layer over the entire corrosion surface to slow down the release after first few days. Therefore, the UFG structure is able to minimize the burst release of Cu²⁺ [21].

The addition of active Mg into the UFG Cu further eases the burst release. The added Mg and the Cu matrix could form a micro-galvanic cell in which the physically contacted Mg and Cu play the roles of the sacrificed anode and the protected cathode within SUF. Because the electrochemical potential differences of Mg and Cu, -1.54V~-1.59 [37] for Mg and -0.25V [21] for Cu in SUF, respectively, Mg would suffer severe galvanic corrosion [41]. It is not only the Mg that could be used to protect the Cu corrosion, other relative active metals, such as Zn, Sn, Ni, Al, Mn, Ag and Ti in Cu, could also enhance the corrosion resistance of Cu in a variety of environments [21,37,42-44]. Due to the low amount of Mg in Cu, the burst release of the Cu²⁺ was eased to some extent by Mg. The optimized alloying concentration of Mg in Cu needs more systematic study. In this work, we alloyed 0.4 wt.% Mg because of the considerations in Mg solubility in Cu-Mg solid solution [45], the long-term Cu²⁺ release from Cu-IUD, the mechanical properties and the grain size reduction using ECAP and also the balance of the contraceptive efficacy from Cu and the enhancement of cell bioactivity from Mg. Thus, the Mg concentration was kept low in Cu to inhibit the Cu²⁺ burst release together with the UFG struc-

Moreover, the in vitro long-term Cu²⁺ release rate from the UFG Cu-0.4Mg stabilized at 1.93 µg/day after 150 days. The release rate was higher than that either from the CG Cu and or from the UFG Cu, and is more sufficient for long-term antifertility. This might be attributed to the loose corrosion product layer and also micropores formed from the hydrogen evolution [46,47]. The hydrogen evolution from the Mg dissolution, although small amount, could uniformly form the micro-pores, allowing the Cu₂O and also the deposited other corrosion products relatively porous and enabling the Cu²⁺ release through the pores. Neither Mg element nor Mg(OH)₂ was found in the corrosion products of UFG Cu-0.4Mg using EDS and XRD [48]. However, it is found the formed micropores in the corrosion layer and the Mg2+ in the SUF, suggesting the dissolution of Mg. Therefore, we speculated that the reason why the Mg oxidation or oxyhydroxidation was not observed on the implanted UFG Cu-0.4Mg could be possibly because of (1) the added Mg was quite low, only 0.4 wt.% in present study; (2) the dissolution of these products under the particular environment of the uteri; (3) it is possible that these corrosion products present in extremely small amounts and dimension that could be detected by neither XRD nor EDS [48].

The Mg element in UFG Cu also played an important role in enhancing the biocompatibility and comfortability for the Cu-IUD adoption. The side effects from the burst release of Cu²⁺ are eased by the release of Mg²⁺. It is commonly believed that the Cu²⁺ prevent fertilization through a cytotoxic inflammatory reaction which could inhibit the mobility, viability, and implantation of sperm, ovum and early embryo [49,50]. Cu²⁺ could directly bound to or uptake within the sperm cells [51] to ultimately affect their mobility and viability. On the other hand, Cu²⁺ could induce significant endometrial changes, including increased leukocytes, mononuclear cells, neutrophils, and plasma cells in endometrium [52-54], damaged endometrial extracellular matrix [55,56]. These endometrial changes would possibly lead cramping pain and erratic and excessive bleeding. In addition, the excessive Cu2+ could also induce the apoptosis of endometrial stroma cells [57,58] through nonspecifically interactions with intracellular proteins [59], which are

the causes of ultra-bleeding and pain occurred among IUD users [60]. Specifically, the TC50 value of Cu^{2+} to HEEC was 170 μ M (10.88 µg/mL) in 24 h [61] and the decidualization of HESC was significant with Cu^{2+} at 250 μ M (16.0 μ g/mL) [58]. The in vitro cytotoxicity results in Figs. 5, 6 and S7 confirmed that UFG Cu-0.4Mg with reduced Cu²⁺ presented the highest proliferation rate of HEEC, HESC, and HUVEC with all concentrations of Cu²⁺ ions as well as lower expression of inflammation cytokines of IL-1b, IL-6, and IL-8 [62], suggesting less endometrial changes. Moreover, the direct observation on endometrium morphology of rats inserted with UFG Cu-0.4Mg displayed mild inflammatory reaction without obvious morphology and structure alterations at the end of 4weeks' observation. Whereas the significant inflammatory cell infiltration with squamous metaplasia phenomenon of the uterine endothelial cells were observed in both CG Cu and UFG Cu after 14- and 28-days' insertion. An increment in the microvessel density in uterus appeared in the UFG Cu group due to the burst release of Cu^{2+} [63].

Furthermore, elevated serum Cu²⁺ concentrations in the CG Cu and UFG Cu groups were detected in the rats at the early stage after implantation and much reduced amount of Cu²⁺ in serum was found for the rats with UFG Cu-0.4Mg. Previous study had also exhibited that women with the TCu380A IUD displayed significant increase of Cu²⁺ in serum, not reaching toxic criteria three months after TCu-380A IUD insertion [64]. It was reported that a conserved mechanism of Cu tolerance is metal sequestration by metallothioneins (MTs) [65]. Elevated Cu²⁺ levels in the cytoplasm prompt the expression of MTs, thus maintaining the normal level of Cu ion. One study also indicated that MTs along with other Cu regulatory protein possessed capabilities of cellular storage within a certain and specific range of Cu exposure. The precise mechanism of biological copper homeostasis needs further research on giving an acute damage of endometrium induced by excessive amounts of copper.

On the other hand, Mg²⁺ may be able to ease the side effect from the antifertilization of Cu²⁺, like bleeding, cramping and pain. Mg²⁺ has shown beneficial effects on bone cells and tissues [66] from Mg based alloys as orthopedic and cardiovascular implants [67,68]. It is possible for Mg²⁺ to promote the self-healing of the endometrial extracellular matrix. Moreover, Mg²⁺ has been applied in clinic to relax muscle contraction for its spasmolytic properties [69]. Therefore, the released Mg²⁺ would probably ease the uterus muscle cramping along the endometrial changes. The biocompatibility and intolerance of Cu-IUD could be improved to some extent by Mg²⁺ although the exact effect and the optimized Mg²⁺ should be investigated more detailed for UFG Cu-IUD.

It was also found that the corrosion surfaces of Cu materials after in vitro long-term immersion and the in vivo implantation varied a lot. It was reported that IUD in utero could change the structures of endometrium due to the foreign body response [70]. Since the stiff corrosion products adhered to the surface of the corroded materials could induce friction in the interface between them and the endometrium [71]. In these in vivo implantation tests, a much cleaner surface was observed in the UFG Cu-0.4Mg group compared with a course one in the corroded CG Cu. The surface of the UFG Cu is less smooth than the UFG Cu-0.4Mg group with corrosion products deposited non-uniformly. Sulfur-containing compounds were detected on the surface both of CG Cu and UFG Cu. The formation of sulfur-containing compounds on the surface of the Cu materials could probably attributed to the reaction of the albumin with sulfhydryl group (-SH) in rats' fluid [72] with the Cu or Cu²⁺. In addition, the severe inflammation reaction appeared in the endometrium of the CG Cu and UFG Cu group could result in more serum albumin filtrate into the uterine fluid. Similar sulfurcontaining compounds had been observed and report for the Nova-T copper IUDs collected from clinics after over 12 months' implan-

tation in women's utero. It also found that the sulfur-containing compounds became much denser when it was used for over 18 months [73]. All these results demonstrated the improved corrosion resistance and histocompatibility of UFG Cu-0.4Mg with the addition of Mg. More importantly, UFG Cu-0.4Mg performed good antifertility effectiveness.

5. Conclusions

Ultrafine grained bulk copper-magnesium alloy, UFG Cu-0.4Mg, with high density of grain boundaries was developed as the active intrauterine materials. The added Mg in the ultrafine grained Cu matrix could form a micro-galvanic cell in which the physically contacted Mg and Cu play the roles of the sacrificed anode and the protected cathode within SUF, respectively. Mg would suffer severe galvanic corrosion and dissolve earlier than Cu, thus the burst release of the Cu²⁺ was eased. Moreover, the hydrogen evolution from the Mg dissolution enabled the formation of porous corrosion layer allowing sufficient and sustainable Cu2+ release in a long term. Therefore, the UFG Cu-0.4Mg exhibited much eased burst release of Cu²⁺ in the first few days of in vitro immersion tests and higher Cu²⁺ release rate in long-term immersion up to 300 days. The biocompatibility results demonstrated less severe inflammation from the UFG Cu-0.4Mg material to the uterus cells. The in vivo observation of the uterus tissues after UFG Cu-0.4Mg implanted into rats' uteri presented much reduced tissue damage and the compromised inflammatory reaction and recovery of endometrial epithelium. Furthermore, the contraceptive effectiveness of UFG Cu-0.4Mg was well maintained. The ultrafine grained structure and the added Mg alloy element synchronically played an important role in the regulation of Cu²⁺ release and responses to endometrial microenvironment, which both benefits to ease the side effects of Cu-IUD adoption. UFG Cu-0.4Mg has been proved the high potential as a new upgrading or alternative material for intrauterine devices.

Associated Content

The Supporting Information (SI) is provided separately. Summarized tables and detailed XRD, $\mathrm{Cu^{2+}}$ and $\mathrm{Mg^{2+}}$ release profile comparison, corrosion rate calculation and comparison, EDS spectra for implanted Cu materials, as well as XRD patterns for corrosion produced analysis are provided in SI.

Declaration of Competing Interest

The authors declare that they have no known competing financial interests or personal relationships that could have appeared to influence the work reported in this paper.

Acknowledgment

This work was supported by the National Key R&D Program of China (Grant No. 2016YFC1000903), the Nonprofit Central Research Institute Fund of National Research Institute For Family Planning (Grant No. 2020GJZ07). This project was partially supported by the Chancellor Postdoctoral Research Fellowship of University of Technology Sydney (Xiaoxue Xu). We would like to acknowledge the Microscopy Analysis Unit at the University of Technology Sydney for the Electronic Backscatter Diffraction (EBSD) analysis. We thank Dr Jacob Byrnes in the Australian Centre for Microscopy & Microanalysis at the University of Sydney for EBSD sample preparation.

Supplementary material [33]

Supplementary material associated with this article can be found, in the online version, at doi:10.1016/j.actbio.2021.04.037.

References

- D.M. Bastidas, B. Valdez, M. Schorr, J.M. Bastidas, Corrosion of copper intrauterine devices: review and recent developments, Corros. Rev. 37 (4) (2019) 307–320
- [2] K.M. Curtis, J.F. Peipert, Long-acting reversible contraception, N. Engl. J. Med. 376 (5) (2017) 461–468.
- [3] M.K. Findley, E.E. Levi, M.V. Dragoman, Intrauterine devices and contraceptive implants: overview of options and updates on method use, Curr. Obstet. Gynecol. Rep. 6 (2) (2017) 85–93.
- [4] J. Krashin, J.H. Tang, S. Mody, L.M. Lopez, Hormonal and intrauterine methods for contraception for women aged 25 years and younger, Cochrane Database Syst. Rev. (8) (2015) CD009805.
- [5] M.E. Ortiz, H.B. Croxatto, Copper-T intrauterine device and levonorgestrel intrauterine system: biological bases of their mechanism of action, Contraception 75 (6 Suppl) (2007) S16–S30.
- [6] B. Cao, T. Xi, Y. Zheng, Release behavior of cupric ions for TCu380A and TCu220C IUDs, Biomed. Mater. 3 (4) (2008) 044114.
- [7] R. Kulier, P.A. O'Brien, F.M. Helmerhorst, M. Usher-Patel, C. D'Arcangues, Copper containing, framed intra-uterine devices for contraception, Cochrane Database Syst. Rev. (4) (2007) CD005347.
- [8] S. Fadiloglu, B. Dilbaz, E. Fadiloglu, S. Dilbaz, Relationship between copper IUD complications and ultrasonographic findings, Arch. Gynecol. Obstet. 297 (4) (2018) 989–996
- [9] L. Li, J. Li, N. Li, Y. Zhang, X. Feng, Analysis of the reason of abnormal uterine bleeding induced by copper corrosion of IUD Cu, Clin. Exp. Obstet. Gynecol. 43 (6) (2016) 883–886.
- [10] J. Zhou, X. Tan, X. Song, K. Zhang, J. Fang, L. Peng, W. Qi, Z. Nie, M. Li, R. Deng, C. Yan, Temporal trends of copper-bearing intrauterine device discontinuation: a population-based birth-cohort study of contraceptive use among rural married women in China, Asia Pac. J. Public Health 27 (2) (2015) NP2433–NP2442.
- [11] P. Verdugo, R. Latorre, O. Alvarez, M. Medel, D. Benos, Effects of copper and zinc on rat uterine muscle contraction and rabbit blastocyst fluid accumulation, Biol. Reprod. 25 (3) (1981) 502–510.
- [12] E. Wiebe, J. Trussell, Discontinuation rates and acceptability during 1 year of using the intrauterine ball (the SCu380A), Contraception 93 (4) (2016) 364–366.
- [13] F. Alvarez, P.L. Schilardi, M.F. de Mele, Reduction of the "burst release" of copper ions from copper-based intrauterine devices by organic inhibitors, Contraception 85 (1) (2012) 91–98.
- [14] F. Alvarez, C. Grillo, P. Schilardi, A. Rubert, G. Benitez, C. Lorente, M.F. de Mele, Decrease in cytotoxicity of copper-based intrauterine devices (IUD) pretreated with 6-mercaptopurine and pterin as biocompatible corrosion inhibitors, ACS Appl. Mater. Interfaces 5 (2) (2013) 249–255.
- [15] B. Chen, C. Liang, D. Fu, D. Ren, Corrosion behavior of Cu and the Cu-Zn-Al shape memory alloy in simulated uterine fluid, Contraception 72 (3) (2005) 221–224.
- [16] W. Zhang, X. Xia, C. Qi, C. Xie, S. Cai, A porous Cu/LDPE composite for copper-containing intrauterine contraceptive devices, Acta Biomater. 8 (2) (2012) 897–903.
- [17] S. Cai, X. Xia, C. Xie, Corrosion behavior of copper/LDPE nanocomposites in simulated uterine solution, Biomaterials 26 (15) (2005) 2671–2676.
- [18] L. Sun, X.B. Huang, J.P. Suo, B.L. Fan, Z.L. Chen, W.X. Yang, J. Li, Biological evaluation of a novel copper-containing composite for contraception, Fertil. Steril. 95 (4) (2011) 1416–1420.
- [19] Z. Yang, C. Xie, X. Xia, S. Cai, Zn(2+) release behavior and surface characteristics of Zn/LDPE nanocomposites and ZnO/LDPE nanocomposites in simulated uterine solution, J. Mater. Sci. Mater. Med. 19 (11) (2008) 3319–3326.
- [20] Z. Yang, C. Xie, Zn²⁺ release from zinc and zinc oxide particles in simulated uterine solution, Colloids Surf. B Biointerfaces 47 (2) (2006) 140–145.
- [21] X.X. Xu, F.L. Nie, Y.B. Wang, J.X. Zhang, W. Zheng, L. Li, Y.F. Zheng, Effective inhibition of the early copper ion burst release with ultra-fine grained copper and single crystal copper for intrauterine device application, Acta Biomater. 8 (2) (2012) 896-896.
- [22] X.X. Xu, F.L. Nie, J.X. Zhang, W. Zheng, Y.F. Zheng, C. Hu, G. Yang, Corrosion and ion release behavior of ultra-fine grained bulk pure copper fabricated by ECAP in Hanks solution as potential biomaterial for contraception, Mater. Lett. 64 (4) (2010) 524–527.
- [23] D.P. de Oliveira, T.V. Toniato, R. Ricci, F.R. Marciano, E. Prokofiev, R.Z. Valiev, A.O. Lobo, A.M. Jorge Júnior, Biological response of chemically treated surface of the ultrafine-grained Ti-6Al-7Nb alloy for biomedical applications, Int. J. Nanomed. 14 (2019) 1725–1736.
- [24] C.N. Elias, M.A. Meyers, R.Z. Valiev, S.N. Monteiro, Ultrafine grained titanium for biomedical applications: an overview of performance, J. Mater. Res. Technol. 2 (4) (2013) 340–350.
- [25] R.D.K. Misra, W.W. Thein-Han, T.C. Pesacreta, K.H. Hasenstein, M.C. Somani, L.P. Karjalainen, Cellular response of preosteoblasts to nanograined/ultrafine-grained structures, Acta Biomater. 5 (5) (2009) 1455-1467.
- [26] L. Saldaña, A. Méndez-Vilas, L. Jiang, M. Multigner, J.L. González-Carrasco, M.T. Pérez-Prado, M.L. González-Martín, L. Munuera, N. Vilaboa, *In vitro* biocompatibility of an ultrafine grained zirconium, Biomaterials 28 (30) (2007) 4343–4354.
- [27] G. Qiang, E. Mostaed, C. Zanella, Y. Zhentao, M. Vedani, Ultra-fine grained degradable magnesium for biomedical applications, Rare Met. Mater. Eng. 43 (11) (2014) 2561–2566.

- [28] N. Sezer, Z. Evis, S.M. Kayhan, A. Tahmasebifar, M. Koç, Review of magnesium-based biomaterials and their applications, J. Magnes. Alloys 6 (1) (2018) 23-43
- [29] M.J. Laires, C.P. Monteiro, M. Bicho, Role of cellular magnesium in health and human disease, Front. Biosci. 9 (2004) 262–276.
- [30] J.A. Maier, S. Castiglioni, L. Locatelli, M. Zocchi, A. Mazur, Magnesium and inflammation: advances and perspectives, Semin. Cell Dev. Biol. S1084-9521 (20) (2020) 30171–30173.
- [31] E.A. Unwaha, F.A. Bello, O.O. Bello, A. Oladokun, Intravenous magnesium sulfate in the management of severe pre-eclampsia: a randomized study of 12-hour versus 24-hour maintenance dose, Int. J. Gynaecol. Obstet. 149 (1) (2020) 37–42.
- [32] L.A. Wetta, J.M. Szychowski, S. Seals, M.S. Mancuso, J.R. Biggio, A.T. Tita, Risk factors for uterine atony/postpartum hemorrhage requiring treatment after vaginal delivery, Am. J. Obstet. Gynecol. 209 (51) (2013) e1–e6.
- [33] R. Mehdi, H. Yan, Assessment of magnesium-based biomaterials: from bench to clinic, Biomater. Sci. 7 (6) (2019) 2241–2263.
- [34] M.P. Staiger, A.M. Pietak, J. Huadmai, G. Dias, Magnesium and its alloys as orthopedic biomaterials: a review, Biomaterials 27 (9) (2006) 1728–1734.
- [35] J.M. Bastidas, E. Cano, N. Mora, Copper corrosion-simulated uterine solutions, Contraception 61 (6) (2000) 395–399.
- [36] ASTM G1-03Standard Practice for Preparing, Cleaning, and Evaluating Corrosion Test Specimens, ASTM International, Philadelphia West Conshohocken, PA, 2004.
- [37] G. Bao, Q. Fan, D. Ge, M. Sun, H. Guo, D. Xia, Y. Liu, J. Liu, S. Wu, B. He, Y. Zheng, In vitro and in vivo studies on magnesium alloys to evaluate the feasibility of their use in obstetrics and gynecology, Acta Biomater. 97 (2019) 623–636.
- [38] S.S. Pathak, S.K. Mendon, M.D. Blanton, J.W. Rawlins, Magnesium-based sacrificial anode cathodic protection coatings (Mg-rich primers) for aluminum alloys, Metals 2 (3) (2012) 353–376.
- [39] H. Nady, M.M. El-Rabiei, G.M. Abd El-Hafez, Electrochemical stability of Cu-10Al-10Zn, Cu-10Al-10Ni, and Cu-10Ni-10Zn ternary alloys in simulated physiological solutions, J. Bio- Tribo-Corros. 2 (28) (2016) 1-12.
- [40] X. Zhao, Q. Liu, H. Sun, Y. Hu, Z. Wang, Chronic systemic toxicity study of copper intrauterine devices in female Wistar rats, Med. Sci. Monit. 23 (2017) 3961–3970
- [41] Y. Ma, X. Liang, S. Tong, G. Bao, Q. Ren, Z. Dai, Gold nanoshell nanomicelles for potential magnetic resonance imaging, light-triggered drug release, and photothermal therapy, Adv. Funct. Mater. 23 (7) (2013) 815–822.
- [42] M.A. Shaik, K.H. Syed, B.R. Golla, Electrochemical behavior of mechanically alloyed hard Cu-Al alloys in marine environment, Corros. Sci. 153 (2019) 249–257.
- [43] A.M. Alfantazi, T.M. Ahmed, D. Tromans, Corrosion behavior of copper alloys in chloride media, Mater. Des. 30 (7) (2009) 2425–2430.
- [44] H. Wei, L.-f. Hou, Y.-c. Cui, Y.-h. Wei, Effect of Ti content on corrosion behavior of Cu-Ti alloys in 3.5 % NaCl solution, Trans. Nonferrous Met. Soc. China 28 (4) (2018) 669–675.
- [45] A.A. Nayeb-Hashemi, J.B. Clark, The Cu-Mg (copper-magnesium) system, Bull. Alloy Phase Diagr. 5 (1) (1984) 36–43.
- [46] Z. Li, X. Gu, S. Lou, Y. Zheng, The development of binary Mg-Ca alloys for use as biodegradable materials within bone, Biomaterials 29 (10) (2008) 1329-1344.
- [47] X. Gu, Y. Zheng, Y. Cheng, S. Zhong, T. Xi, In vitro corrosion and biocompatibility of binary magnesium alloys, Biomaterials 30 (4) (2009) 484–498.
- [48] D. Wildemeersch, P.J. Sabbe, M.G. Dowsett, V. Flexer, P. Thompson, D. Walker, P.A. Thomas, A. Adriaens, Assessment of copper corrosion from frameless copper IUDs after long-term in utero residence, Contraception 90 (4) (2014) 454-459.
- [49] J.B. Stanford, R.T. Mikolajczyk, Mechanisms of action of intrauterine devices: update and estimation of postfertilization effects, Am. J. Obstet. Gynecol. 187 (6) (2002) 1699–1708.
- [50] O.A. Adeyemi-Fowode, J.L. Bercaw-Pratt, Intrauterine devices: effective contraception with noncontraceptive benefits for adolescents, J. Pediatr. Adolesc. Gynecol. 32 (5S) (2019) S2–S6.
- [51] M.K. Holland, I.G. White, Heavy metals and human spermatozoa. III. The toxicity of copper ions for spermatozoa, Contraception 38 (6) (1988) 685–695.
- [52] G.K. Oster, Chemical reactions of the copper intrauterine device**supported by the ford foundation, grant 6900106, Fertil. Steril. 23 (1) (1972) 18–23.

- [53] D.R. Mishell, Intrauterine devices: mechanisms of action, safety, and efficacy, Contraception 58 (3) (1998) 45S-53S.
- [54] B. Kaneshiro, T. Aeby, Long-term safety, efficacy, and patient acceptability of the intrauterine copper T-380A contraceptive device, Int. J. Women's Health 2 (2010) 211–220.
- [55] J. Skrzypczak, P. Wirstlein, M. Mikolajczyk, Could the defects in the endometrial extracellular matrix during the implantation be a cause for impaired fertility? Am. J. Reprod. Immunol. 57 (1) (2007) 40–48.
- [56] L.X. Hu, H. Wang, M. Rao, X.L. Zhao, J. Yang, S.F. Hu, J. He, W. Xia, H. Liu, B. Zhen, H. Di, C. Xie, X. Xia, C. Zhu, Alterations in the endometrium of rats, rabbits, and Macaca mulatta that received an implantation of copper/low-density polyethylene nanocomposite, Int. J. Nanomed. 9 (2014) 1127–1138.
- [57] J.P. Carrascosa, D. Cotan, I. Jurado, M. Oropesa-Avila, P. Sanchez-Martin, R.F. Savaris, J. Tan, J.A. Sanchez-Alcazar, S.L. Tan, J.A. Horcajadas, The effect of copper on endometrial receptivity and induction of apoptosis on decidualized human endometrial stromal cells, Reprod. Sci. 25 (7) (2018) 985–999.
- [58] Y. Li, Z.L. Kang, N. Qiao, L.M. Hu, Y.J. Ma, X.H. Liang, J.L. Liu, Z.M. Yang, Effects of excess copper ions on decidualization of human endometrial stromal cells, Biol. Trace Elem. Res. 177 (1) (2017) 10–15.
- [59] C.A. Grillo, M.A. Reigosa, M.A. Fernández Lorenzo de Mele, Does over-exposure to copper ions released from metallic copper induce cytotoxic and genotoxic effects on mammalian cells? Contraception 81 (4) (2010) 343–349.
- [60] J.N. Sanders, D.E. Adkins, S. Kaur, K. Storck, L.M. Gawron, D.K. Turok, Bleeding, cramping, and satisfaction among new copper IUD users: a prospective study, PLoS ONE 13 (11) (2018) e0199724.
- [61] J. Wu, L. Wang, J. He, C. Zhu, *In vitro* cytotoxicity of Cu(2)(+), Zn(2)(+), Ag(+) and their mixtures on primary human endometrial epithelial cells, Contraception 85 (5) (2012) 509–518.
- [62] A. Luckow Invitti, E. Schor, R. Martins Parreira, A. Kopelman, G. Kamergorodsky, G.A. Goncalves, M.J. Batista Castello Girao, Inflammatory cytokine profile of cocultivated primary cells from the endometrium of women with and without endometriosis, Mol. Med. Rep. 18 (2) (2018) 1287–1296.
- [63] J. Li, Z. Liu, S. Li, C. Xie, Y. Duan, J. Yu, C. Zhu, Correlative investigation of copper/low-density polyethylene nanocomposite on the endometrial angiogenesis in rats, Front. Med. China 1 (4) (2007) 401–404.
- [64] S. Imani, L. Moghaddam-Banaem, S. Roudbar-Mohammadi, M. Asghari-Ja-farabadi, Changes in copper and zinc serum levels in women wearing a copper TCu-380A intrauterine device, Eur. J. Contracept. Reprod. Health Care 19 (1) (2014) 45–50.
- [65] J. Calvo, H. Jung, G. Meloni, Copper metallothioneins, IUBMB Life 69 (4) (2017) 236–245.
- [66] C.M. Serre, M. Papillard, P. Chavassieux, J.C. Voegel, G. Boivin, Influence of magnesium substitution on a collagen-apatite biomaterial on the production of a calcifying matrix by human osteoblasts, J. Biomed. Mater. Res. 42 (4) (1998) 626–633.
- [67] N. Li, Y. Zheng, Novel magnesium alloys developed for biomedical application: a review, J. Mater. Sci. Technol. 29 (6) (2013) 489–502.
- [68] Y. Li, L. Liu, P. Wan, Z. Zhai, Z. Mao, Z. Ouyang, D. Yu, Q. Sun, L. Tan, L. Ren, Z. Zhu, Y. Hao, X. Qu, K. Yang, K. Dai, Biodegradable Mg-Cu alloy implants with antibacterial activity for the treatment of osteomyelitis: in vitro and in vivo evaluations, Biomaterials 106 (2016) 250–263.
- [69] J.E. Irazuzta, N. Chiriboga, Magnesium sulfate infusion for acute asthma in the emergency department, Jornal De Pediatria 93 (2017) 19–25.
- [70] K. Patai, L. Devenyi, R. Zelko, Comparison of surface morphology and composition of intrauterine devices in relation to patient complaints, Contraception 70 (2) (2004) 149–152.
- [71] S. Hu, Y. Wang, D. Ke, F. Zhou, G. Cheng, W. Xia, C. Zhu, Antifertility effectiveness of a novel copper-containing intrauterine device material and its influence on the endometrial environment in rats, Mater. Sci. Eng. C Mater. Biol. Appl. 89 (2018) 444–455.
- [72] I. Ringler, The composition of rat uterine luminal fluid, Endocrinology 68 (1961) 281–291.
- [73] E. Chantler, P. Kenway, Z. Larouk, E.B. Faragher, J. Morris, A. Kosonen, H. Allonen, M. Elstein, An analysis of the corrosion process of the Nova-T IUD, Adv. Contracept. 10 (4) (1994) 287–301.